Physical Principles of Spin Pumping

35

Saburo Takahashi

Contents

Abstract

The spin pumping is a versatile method to create the spin current and spin accumulation in various conducting materials in hybrid nanostructures. In this chapter a theoretical description for spin pumping from a ferromagnet into a normal metal is presented based on the spin-exchange interaction between localized moments and conduction electrons in hybrid nanostructures. It is demonstrated that pure spin currents are generated by the coherent spin pumping

S. Takahashi (✉)
Institute for Materials Research, Tohoku University, Sendai, Japan
e-mail: takahasi@imr.tohoku.ac.jp

Y. Xu et al. (eds.), *Handbook of Spintronics*,
DOI 10.1007/978-94-007-6892-5_51

due to ferromagnetic resonance and the thermal spin pumping due to the spin Seebeck effect. The inverse effect that the spin dynamics is manipulated by spin injection into a ferromagnet from a normal metal with strong spin-orbit coupling using the spin-Hall effect is also discussed.

Introduction

There has been growing interest in the phenomena caused by the interplay between spin-dependent transport and magnetization dynamics of ferromagnets in hybrid nanostructures [1, 2]. This is not only because new spin transport phenomena emerge but also because the potential applications to spin-based magnetoelectronic devices are expected [3]. Recent extensive experimental and theoretical studies have demonstrated that nonequilibrium spin injection from a ferromagnet into a nonmagnetic material creates spin current and spin accumulation in various nonmagnetic materials.

Spin current is a flow of spin angular momentum carried by conduction electrons in normal and ferromagnetic metals or by spin waves (magnons) in ferromagnets [4]. Spin angular momentum transfer plays a central role both in magnetization switching caused by spin-transfer torque and in spin pumping caused by magnetization precession. Spin current without accompanying charge current, the so-called pure spin current, is particularly important for spintronic applications because of reducing heat dissipation and is created in nonmagnetic materials by the methods, e.g., nonlocal spin injection [5–11], spin pumping [12–17], and the spin-Hall effect [18–29]. The efficient spin injection, spin transfer, spin manipulation, and spin detection are of crucial importance in utilizing the spin degrees of freedom as a new functionality in spin-based magnetoelectronic devices.

Spin pumping is a method to generate a spin current (spin accumulation) from a ferromagnet into an adjacent metal or semiconductor in hybrid structures using magnetization dynamics, such as magnetization precession caused by ferromagnetic resonance (FMR) [12–17, 21]. In FMR, spin angular momentum is steadily transferred from externally applied microwaves, via the precession of magnetization driven by microwave, to the ferromagnetic material, in which the rate of spin angular momentum supplied from microwave fields to the magnetization is balanced with the rate of magnetization damping (the so-called Gilbert damping) at which the spin angular momentum is dissipated to the lattice. When a normal conductor is electrically in contact with a ferromagnet with the precessing magnetization, the spin angular momentum can flow out of the ferromagnet into the normal conductor through the interface, resulting in the creation of spin current and the enhanced magnetization damping. It is also possible to generate a spin current by thermal effects using heat flow or temperature difference in nanostructures [30, 31]. The spin pumping is widely used as a versatile spin-injection method to create spin current and spin accumulation in various conducting materials in hybrid nanostructures.

In this chapter, a theoretical description of spin pumping based on the spin-exchange interaction between localized moments and conduction electrons in hybrid nanostructures is presented. This gives an alternative approach to the spin-pumping formalism [32–34] based on the Landauer-Büttiker scattering formalism [35, 36]. These approaches are complementary to each other and provide a deeper understanding of the physics of spin pumping.

Basic Equations

A ferromagnetic metal is phenomenologically modeled as a system of localized moments (*d*-electrons) and conduction electrons (*s*-electrons), which are coupled by the exchange interaction [12, 13, 37–40]. The localized moments mainly carry the magnetization of ferromagnet, and the conduction electrons mainly carry charge and spin current. The system is described by the Hamiltonian $H = H_0 + H_{sd} + H_z$, where H_0 consists of the Hamiltonians of conduction electrons and localized moments and H_{sd} represents the so-called *s-d* exchange interaction between them [37–41]:

$$H_{sd} = -J_{sd} v_a \int d\mathrm{r} \hat{\mathbf{S}}(\mathbf{r}, t) \cdot \hat{\mathbf{s}}(\mathbf{r}, t). \tag{1}$$

Here J_{sd} is the exchange interaction constant, v_a is the volume per lattice site, and $\hat{\mathbf{S}}(\mathbf{r}, t)$ and $\hat{\mathbf{s}}(\mathbf{r}, t)$ are, respectively, the spin densities of localized spins and conduction electrons,

$$\hat{\mathbf{S}}(\mathbf{r}, t) = \sum \hat{\mathbf{S}}_i(t) \delta(\mathbf{r} - \mathbf{r}_i), \tag{2}$$

$$\hat{\mathbf{s}}(\mathbf{r}, t) = \sum_{\sigma' \sigma} \psi^{\dagger}_{\sigma'}(\mathbf{r}, t) \hat{\mathbf{s}}_{\sigma' \sigma} \psi_{\sigma}(\mathbf{r}, t), \tag{3}$$

where $\hat{\mathbf{S}}_i$ is localized spin at lattice site i ($|\mathbf{S}_i| = S$), $\hat{\mathbf{s}}_{\sigma' \sigma}$ is electron spin operator, and $\psi^{\dagger}_{\sigma}$ and ψ_{σ} are the creation and annihilation operators of conduction electrons with spin $\sigma(=\uparrow, \downarrow)$. The Hamiltonian H_Z is of the Zeeman type

$$H_{\mathrm{Z}} = \gamma \hbar \int d\mathrm{r} \hat{\mathbf{S}}(\mathbf{r}, t) \cdot \mathbf{H}_{eff} + \gamma_e \hbar \int d\mathbf{r} \hat{\mathbf{s}}(\mathbf{r}, t) \cdot \mathbf{H}, \tag{4}$$

where $\mathbf{H}_{\mathrm{eff}}$ is an effective magnetic field acting on localized spins, which includes external dc magnetic field $\mathbf{H}$, microwave field $\mathbf{h}_{ac}(t)$, demagnetization field, and magnetocrystalline anisotropy field; $\gamma = g\mu_{\mathrm{B}}/\hbar$ and $\gamma_e = g_e \mu_{\mathrm{B}}/\hbar$ are the gyromagnetic ratios of localized spin and conduction-electron spin, respectively; g and g_e are the g factors; and μ_{B} is the Bohr magneton.

The equation of motion $d\hat{\mathbf{S}}/dt = i\hbar^{-1}[H, \hat{\mathbf{S}}]$ for the localized spins yields

$$\frac{\partial}{\partial t}\mathbf{M}(\mathbf{r},t) = -\gamma \mathbf{M}(\mathbf{r},t) \times \mathbf{H}_{\text{eff}} - \gamma J_{\text{ex}} \mathbf{M}(\mathbf{r},t) \times \mathbf{m}(\mathbf{r},t), \tag{5}$$

where $\mathbf{M}(\mathbf{r},t) = -\gamma\hbar\left\langle \hat{\mathbf{S}}(\mathbf{r},t) \right\rangle$ is the magnetizations of localized spins, $J_{\text{ex}} = v_a J_{sd}/(\hbar^2 \gamma\gamma_e)$ is the dimensionless exchange interaction constant, and $\mathbf{m}(\mathbf{r},t) = -\gamma\hbar\langle\hat{\mathbf{s}}(\mathbf{r},t)\rangle$ is the magnetization of conduction electrons.

The equation of motion $d\hat{\mathbf{s}}/dt = i\hbar^{-1}[H, \hat{\mathbf{s}}]$ for the conduction-electron spins leads to

$$\frac{\partial}{\partial t}\mathbf{m}(\mathbf{r},t) = -\gamma_e \mathbf{m}(\mathbf{r},t) \times \mathbf{H} - \gamma_e J_{\text{ex}} \mathbf{m}(\mathbf{r},t) \times \mathbf{M}(\mathbf{r},t) + \nabla \cdot \mathbf{j}_m(\mathbf{r},t), \tag{6}$$

where $\mathbf{j}_m(\mathbf{r}, t)$ is the current density of spin magnetic moments given by the expectation value of the current operator

$$\hat{\mathrm{j}}_m(\mathbf{r},t) = -\gamma_e \hbar \sum_{\sigma\sigma'} \mathrm{Re}\left[\psi^{\dagger}_{\sigma'}(\mathbf{r},t)\hat{\mathbf{s}}_{\sigma'\sigma}\left(\frac{\hbar\nabla}{im_e}\right)\psi_{\sigma}(\mathbf{r},t)\right], \tag{7}$$

where m_e is the mass of conduction electrons. The spin-angular-momentum current density $\mathbf{j}_s$ is given by $\mathbf{j}_s = \gamma_e^{-1}\mathbf{j}_m$. The spin current $\mathbf{j}_s$ is a second-order tensor j_{si}^{k} specified by the flow direction i and the spin polarization direction k. Both $\mathbf{j}_s$ and $\mathbf{j}_m$ are called "spin current" in the following.

Landau-Lifshitz-Gilbert Equation and Bloch Equation

In ferromagnets, the localized spins are tightly coupled together by strong exchange interaction to align parallel to each other, which allows one to describe the localized spins in terms of the magnetization $\mathbf{M}$. When a ferromagnet is subject to externally applied microwave $\mathbf{h}_{ac}(t)$ in addition to external dc magnetic field $\mathbf{H}$, the magnetization (the localized spins as a whole) is driven by $\mathbf{h}_{ac}(t)$ away from its equilibrium direction and coherently precess around the direction of $\mathbf{H}$ with fixed magnitude.

The dynamics of magnetization $\mathbf{M}(\mathbf{r}, t)$ is phenomenologically described by including the Gilbert damping term that determines the magnetization dissipation in Eq. 5, which is called the Landau-Lifshitz-Gilbert (LLG) equation [42].

$$\begin{aligned}\frac{\partial}{\partial t}\mathbf{M}(\mathbf{r},t) &= -\gamma \mathbf{M}(\mathbf{r},t) \times [\mathbf{H} + \mathbf{h}_{ac}(t)] - \gamma J_{\text{ex}} \mathbf{M}(\mathbf{r},t) \times \mathbf{m}(\mathbf{r},t) \\ &+ \frac{\alpha_0}{M_s}\left[\mathbf{M}(\mathbf{r},t) \times \frac{\partial}{\partial t}\mathbf{M}(\mathbf{r},t)\right],\end{aligned} \tag{8}$$

where α_0 is the dimensionless Gilbert damping parameter in the absence of the *s-d* exchange interaction and $M_s = |\mathbf{M}(\mathbf{r}, t)| = \hbar\gamma S/v_a$ is the saturation magnetization. For simplicity, demagnetization and magnetocrystalline anisotropy fields are disregarded, as they are much weaker than the exchange interaction.

The dynamics of the magnetization $\mathbf{m}(\mathbf{r}, t)$ of conduction electrons is phenomenologically described by including the spin relaxation term in Eq. 6 and assuming the diffusive spin current $\mathbf{j}_m = -D\nabla\mathbf{m}$, where D is the diffusion constant of conduction electrons, which results in the Bloch equation with the diffusion term [43, 44].

$$\frac{\partial \mathbf{m}(\mathbf{r}, t)}{\partial t} = -\gamma_e \mathbf{m}(\mathbf{r}, t) \times J_{\mathrm{ex}} \mathbf{M}(\mathbf{r}, t) - \frac{\partial \mathbf{m}(\mathbf{r}, t)}{\tau_{\mathrm{sf}}} + D\nabla^2 \mathbf{m}(\mathbf{r}, t), \tag{9}$$

where τ_{sf} is the spin relaxation time, $\delta\mathbf{m}(\mathbf{r}, t) = \mathbf{m}(\mathbf{r}, t) - \mathbf{m}_0(\mathbf{r}, t)$ is the nonequilibrium spin (magnetic moment) accumulation, a deviation of $\mathbf{m}(\mathbf{r}, t)$ from the equilibrium local and instantaneous value $\mathbf{m}_0(\mathbf{r}, t) = m_0[\mathbf{M}(\mathbf{r}, t)/M_s]$ induced by exchange field $J_{\mathrm{ex}}\mathbf{M}(\mathbf{r}, t)$ with magnitude $m_0 = \chi_e J_{\mathrm{ex}} M_s$ in the direction of $\mathbf{M}(\mathbf{r}, t)$, $\chi_e = 2\mu_{\mathrm{B}}^2 N(0)$ is the paramagnetic susceptibility of conduction electrons, and $N(0)$ is the density of states at the Fermi level. Note that $m_0/M_s = \chi_e J_{\mathrm{ex}} = (1/2)(\gamma_e/\gamma) J_{sd} v_a N(0) \sim J_{sd}/\varepsilon_{\mathrm{F}}$, where ε_{F} is the Fermi energy. In Eq. 9, the terms due to applied dc and microwave fields are disregarded, unless applied fields play a significant role as in the Hanle dephasing effect [12].

Modeling of Ferromagnetic Layer

It is convenient to decompose the magnetization $\mathbf{M}(\mathbf{r}, t)$ into an array of ferromagnetic sheet magnetization $\mathbf{M}_n(t)$ of atomic layers at position $x_n = na$ using the δ-function: $\mathbf{M}(x, t) = \sum_n \mathbf{M}_n(t)\delta(x - x_n)$. When all the sheet magnetizations uniformly precess in the same phase as in the ferromagnetic resonance (FMR), the magnetization is given by

$$\mathbf{M}(x, t) = \mathbf{M}_a(t) \sum_n \delta(x - x_n), \tag{10}$$

where $\mathbf{M}_a(t) = -\gamma\hbar\mathbf{S}(t)/a^2$ is the sheet magnetization (magnetic moment per area), $\mathbf{S}(t)$ is localized spin at the lattice site, and a is the lattice constant. A ferromagnetic layer is described by an array of ferromagnetic sheets immersed in a free electron gas of a normal metal, and a nonmagnetic layer is simply described by the region in the absence of magnetization sheets. This modeling enables one to solve the coupled equations for $\mathbf{M}(t)$ and $\mathbf{m}(\mathbf{r}, t)$ analytically and numerically in hybrid structures consisting of a ferromagnetic layer and a nonmagnetic layer with comparable spin-diffusion lengths, such as transition metal ferromagnets and heavy noble metals of Pt and Pd, and provides clear physical insight into spin-pumping phenomena.

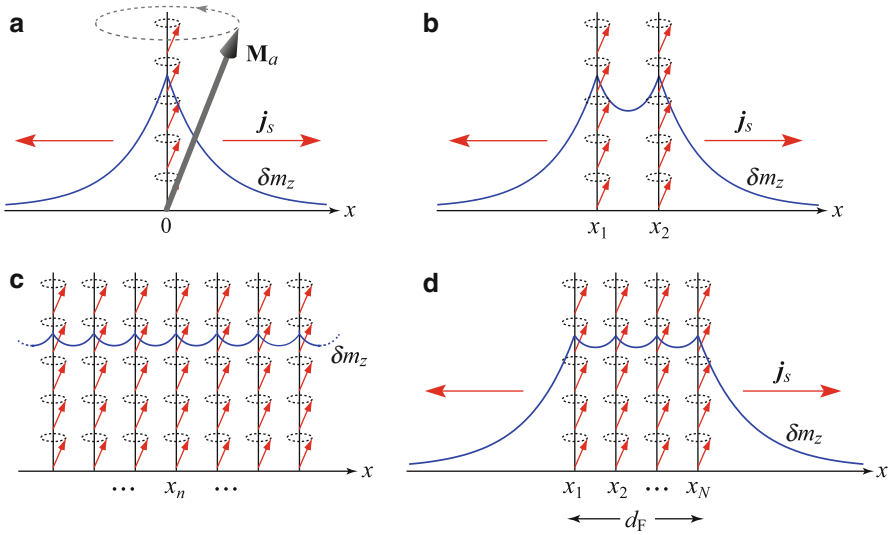

Fig. 1 Spin pumping from ferromagnetic sheets immersed in an electron gas of normal metal (Fermi sea): (**a**) single ferromagnetic sheet at $x = 0$. (**b**) Two ferromagnetic sheets at $x = x_1, x_2$. (**c**) Periodic array of ferromagnetic sheets at $x = x_n = nd$ with period d. (**d**) Array of N ferromagnetic sheets corresponding to a ferromagnetic layer (F) of thickness $d_F = Na$. Each sheet consists of ferromagnetically aligned moments $-\gamma\hbar\mathbf{S}$ indicated by precessing *arrows* and carries the two-dimensional magnetization $\mathbf{M}_a = -\gamma\hbar\mathbf{S}/a^2$. Spin accumulation $\delta\mathbf{m}(x, t)$ and spin current $\mathbf{j}_s(x, t)$ are generated by the uniformly precessing moments represented by *arrows* on the sheets

Spin Pumping by Precessing Magnetizations

A simple description of spin pumping, i.e., how the angular momentum of applied microwave is transferred to conduction electrons to create spin accumulation and spin current via the precession of localized spins, is presented by introducing two-dimensional sheets of localized spins in a normal metal as shown in Fig. 1. A most simple description is spin pumping from a single ferromagnetic sheet, which is pedagogical to capture the fundamental features of spin pumping.

Spin Pumping from a Single Ferromagnetic Sheet

A two-dimensional sheet of ferromagnetically aligned spins of localized electrons (d-electrons) in the yz plane is introduced in an electron gas system of normal metal as shown in Fig. 1a, in which the localized spins in the sheet couple with the conduction electrons (s-electrons) by the exchange interaction. The magnetization of the sheet is represented by the two-dimensional δ-function at $x = 0$,

$$\mathbf{M}(x, t) = \mathbf{M}_a(t)\delta(x) = \mathbf{M}(t)a\delta(x), \tag{11}$$

where $\mathbf{M}(t) = \mathbf{M}_a(t)/a = -\hbar\gamma\mathbf{S}(t)/a^3$ corresponds to a bulk magnetization in the regular array of sheets with lattice period a.

Since the precession frequency ($\omega \sim$ GHz) is much smaller than the spin relaxation rate $\left(\tau_{\rm sf}^{-1} \sim 10^{12}{\rm s}^{-1}\right)$, i.e., $\omega\tau_{\rm sf} \gg 1$, the time derivative term in Eq. 9 is disregarded, so that the Bloch equation becomes the stationary diffusion equation with the source term

$$\left(\frac{1}{\tau_{\rm sf}} - D\nabla^2\right)\delta\mathbf{m}(x,t) = \frac{1}{\tau_{\rm ex}}\left[\hat{\mathbf{M}}(t)\times\delta\mathbf{m}(0,t) - \frac{\chi_e}{\gamma_e}\frac{\partial}{\partial t}\hat{\mathbf{M}}(t)\right]a\delta(x), \tag{12}$$

where $\hat{\mathbf{M}} = \mathbf{M}/M_s = \mathbf{M}_a/M_a = \mathbf{S}/S$ is the magnetization direction and $\tau_{\rm ex} = a/(\gamma_e J_{\rm ex} M_a) = \hbar/(SJ_{sd})$. Equation 12 is integrated as

$$\delta\mathbf{m}(x,t) = \frac{\tau_{\rm sf}}{\tau_{\rm ex}}\frac{a}{2\lambda_s}\left[\hat{\mathbf{M}}(t)\times\delta\mathbf{m}(0,t) - \frac{\chi_e}{\gamma_e}\frac{\partial\hat{\mathbf{M}}(t)}{\partial t}\right]e^{-|x|}/\lambda_s, \tag{13}$$

where $\lambda_s = (D\tau_{\rm sf})^{1/2}$ is the spin-diffusion length. By taking the cross product of $\hat{\mathbf{M}}(t)$ and Eq. 13 at $x = 0$ and using vanishing product $\delta\mathbf{m}(0, t)\cdot\ \hat{\mathbf{M}} = 0$, one obtains

$$\delta\mathbf{m}(x,t) = -\frac{\chi_e}{\gamma_e}\left[\frac{1}{1+\Gamma_a^2}\left(\hat{\mathbf{M}}\times\frac{\partial\hat{\mathbf{M}}}{\partial t}\right) + \frac{\Gamma_a}{1+\Gamma_a^2}\frac{\partial\hat{\mathbf{M}}}{\partial t}\right]e^{-|x|}/\lambda_s, \tag{14}$$

where

$$\Gamma_a = \frac{\tau_{\rm ex}}{\tau_{\rm sf}}\frac{2\lambda_s}{a} = \left(\frac{\hbar}{SJ_{sd}\tau_{\rm sf}}\right)\frac{2\lambda_s}{a}, \tag{15}$$

which indicates that Γ_a in a single sheet is enhanced by the factor $(2\lambda_s/a)$ compared with $\Gamma_{\rm bulk} = \hbar/(SJ_{sd}\tau_{\rm sf})$ in a bulk ferromagnet [39]. As seen in Eq. 14, the parameter Γ_a plays an important role in spin pumping and magnetization dynamics.

Inserting Eq. 14 into the LLG equation, the effective LLG equation is written as

$$\frac{\partial\hat{\mathbf{M}}(t)}{\partial t} = -\widetilde{\gamma}\hat{\mathbf{M}}(t)\times[\mathbf{H} + \mathbf{h}_{ac}(t)] + \alpha\hat{\mathbf{M}}(t)\times\frac{\partial}{\partial t}\hat{\mathbf{M}}(t), \tag{16}$$

with the renormalized parameters [14, 39],

$$\alpha = \frac{\widetilde{\gamma}}{\gamma}(\alpha_0 + \alpha_{\rm SP}),\quad \widetilde{\gamma} = \frac{\gamma}{1+\alpha_{\rm SP}/\Gamma_a}, \tag{17}$$

where $\alpha_{\rm SP}$ is the additional contribution to the Gilbert damping due to spin pumping,

$$\alpha_{\rm SP} = \frac{\gamma}{\gamma_e}\chi_e J_{\rm ex}\frac{\Gamma_a}{1+\Gamma_a^2} = \frac{\hbar\gamma}{2\pi M_a}\left(\frac{h}{2e^2}\frac{1}{\rho_{\rm N}\lambda_s}\right)\frac{1}{1+\Gamma_a^2}, \tag{18}$$

and $\rho_{\rm N} = 1/[2e^2N(0)D]$ is the electrical resistivity. Typical parameter values of $\rho_{\rm N} = 20\mu\Omega$ cm, $\lambda_s = 10$ nm, $a = 0.3$ nm, and $S = 2$ give $\alpha_{\rm SP} \sim 0.05$ in the single ferromagnetic sheet.

The magnetization current $\mathbf{j}_{mx} = -D\nabla_x\delta\mathbf{m}$ pumped by precessing magnetization is

$$\mathbf{j}_{mx}(x,t) = \frac{1}{2}\frac{x}{|x|}\frac{\gamma_e}{\gamma}\alpha' M_a\left(\hat{\mathbf{M}}\times\frac{\partial\hat{\mathbf{M}}}{\partial t} + \Gamma_a\frac{\partial\hat{\mathbf{M}}}{\partial t}\right)e^{-|x|}/\lambda_s \tag{19}$$

the z-component of which is stationary (time independent) spin current and satisfies

$$\left(j_{mx}^z\right)_{\rm pump} = j_{mx}^z(0^+) - j_{mx}^z(0^-) = -\frac{\gamma_e}{\gamma}\alpha_{\rm SP}M_a\left(\hat{\mathbf{M}}\times\frac{\partial\hat{\mathbf{M}}}{\partial t}\right)_z. \tag{20}$$

When circularly polarized microwave $\mathbf{h}(t) = h_{ac}(\cos\omega t, \sin\omega t, 0)$ is applied in the presence of dc magnetic field $\mathbf{H} = (0, 0, H)$, the magnetization is uniformly precessed around the dc magnetic field with circular precession of the transverse components

$$M_\pm(t) = M_x(t) \pm iM_y(t) = M_\pm(0)e^{\pm i\omega t}, \tag{21}$$

$$m_\pm(x,t) = m_x(x,t) \pm im_y(x,t) = m_\pm(x,0)e^{\pm i\omega t}, \tag{22}$$

driven by circularly polarized microwave field $h_\pm(t) = h_x(t) \pm ih_y(t) = h_{ac}e^{\pm i\omega t}$ in the complex representation. For small-angle precession of $\mathbf{M}$, Eq. 16 gives the solutions

$$\hat{M}_\pm(t) = -\frac{\widetilde{\gamma}h_{ac}e^{\pm i\omega t}}{(\omega-\widetilde{\gamma}H)\mp i\alpha\omega}, \tag{23}$$

yielding the FMR lineshape

$$\left(\hat{\mathbf{M}}\times\frac{\partial\hat{\mathbf{M}}}{\partial t}\right)_z = \omega\left[\hat{M}_+(t)\hat{M}_-(t)\right] = \frac{\omega(\widetilde{\gamma}h_{ac})^2}{(\omega-\widetilde{\gamma}H)^2+(\alpha\omega)^2}. \tag{24}$$

At resonance ($\omega = \widetilde{\gamma}H$), the stationary components of spin accumulation and spin current are

$$\delta m_z(x) = -2\pi\frac{\mu_{\rm B}S}{a^2}[\hbar\omega N(0)]\left(\frac{\rho_{\rm N}\lambda_s}{h/2e^2}\right)\alpha_{\rm SP}\sin^2\Theta e^{-|x|}/\lambda_s, \tag{25}$$

$$j_{mx}^{z}(x) = \frac{x}{|x|}\frac{\mu_B S}{a^2}\alpha_{SP}\omega \sin^2\Theta e^{-|x|}/\lambda_s, \tag{26}$$

where Θ is the precession angle of magnetization satisfying $\sin\Theta = (\tilde{\gamma}h_{ac}/\alpha\omega)$.

The microwave absorption power is $P = \left\langle \mathbf{h}(t)\cdot\partial\mathbf{M}_a(t)/\partial t)\right\rangle = \omega \mathrm{Im}\left[h_{ac}^{+}(t)M_a^{-}(t)\right]$, which is combined with the z-component of the LLG equation in Eq. 16 to yield

$$P = M_a\frac{\alpha\omega^2}{\tilde{\gamma}}\left[\hat{M}_+(t)\hat{M}_-(t)\right] = \hbar\omega\frac{S}{a^2}\frac{(\tilde{\gamma}/\gamma)(\gamma h_{ac})^2\alpha\omega}{(\omega-\tilde{\gamma}H)^2+(\alpha\omega)^2}, \tag{27}$$

which becomes $P = \hbar\omega(S/a^2)(\tilde{\gamma}/\gamma)\alpha\omega\sin^2\Theta = a\tilde{\gamma}M_s h_{ac}^2/\alpha$ at resonance.

Spin Pumping from the Periodic Array of Ferromagnetic Sheets

A periodic array of F sheets with arbitrary period d in a normal metal shown in Fig. 1c is studied to see how spin pumping takes place from the F sheets to the conduction electrons, depending on the sheet separation relative to the spin-diffusion length. When all the sheet magnetizations are coherently precessed (in-phase) by microwave, the magnetizations are represented by the periodic array of the two-dimensional δ-functions at $x_n = nd$ with arbitrary sheet separation d,

$$\mathbf{M}(x,t) = \mathbf{M}_a(t)\sum_{n=-\infty}^{\infty}\delta(x-nd). \tag{28}$$

In this case, the Bloch equation Eq. 9 is solved analytically to yield $\delta\mathbf{m}(x, t)$ in a periodic function of x with period d, which reads in a region of $0 < x < d$,

$$\delta\mathbf{m}(x,t) = \frac{\chi_e}{\gamma_e}\frac{1}{1+\Gamma^2}\left(\hat{\mathbf{M}}\times\frac{\partial\hat{\mathbf{M}}}{\partial t}+\Gamma\frac{\partial\hat{\mathbf{M}}}{\partial t}\right)\frac{\cosh[(x-d/2)/\lambda_s]}{\cosh(d/2\lambda_s)}, \tag{29}$$

where

$$\Gamma = \Gamma_a\tanh(d/2\lambda_s), \tag{30}$$

which indicates that Γ strongly depends on the sheet separation relative to the spin-diffusion length. When d is much smaller than λ_s ($d \ll \lambda_s$), $\Gamma \approx (d/2\lambda_s)\Gamma_a$, indicating that Γ is significantly smaller than Γ_a of the single sheet case due to the exchange of spin current between the sheets, whereas when d is much larger than λ_s ($d \gg \lambda_s$), the situation is the same as in the isolated single sheet case ($\Gamma \approx \Gamma_a$).

Using Eq. 29 in Eq. 8, the LLG equation for the magnetization vector $\hat{\mathbf{M}}$ is written in an effective form

$$\frac{\partial}{\partial t}\hat{\mathbf{M}}(t) = -\widetilde{\gamma}\hat{\mathbf{M}}(t) \times (\mathbf{H}_{\text{eff}} + \mathbf{h}_{ac}) + \alpha\left[\hat{\mathbf{M}}(t) \times \frac{\partial \hat{\mathbf{M}}(t)}{\partial t}\right], \tag{31}$$

with the renormalized parameters

$$\alpha = \frac{\widetilde{\gamma}}{\gamma}(\alpha_0 + \alpha_{\text{SP}}), \quad \widetilde{\gamma} = \frac{\gamma}{1 + \alpha_{\text{SP}}/\Gamma}, \tag{32}$$

where

$$\alpha_{\text{SP}} = \chi_e J_{\text{ex}} \frac{\gamma}{\gamma_e} \frac{\Gamma}{1 + \Gamma^2} = \frac{\hbar\gamma}{2\pi M_s a} \frac{g_{\text{N}}^s \tanh(d/2\lambda_s)}{1 + \Gamma_a^2 \tanh^2(d/2\lambda_s)}, \quad g_{\text{N}}^s = \frac{(h/2e^2)}{\rho_{\text{N}}\lambda_s}. \tag{33}$$

Thus, the additional Gilbert damping depends on the separation of the sheets relative to the spin-diffusion length. For $(d/2\lambda_s) \ll 1$, α_{SP} is strongly reduced by the factor $(d/2\lambda_s)$ compared with that of single F sheet, due to the mutual interference between the F sheets through emission and absorption of spin current. For $(d/2\lambda_s) \gg 1$, the sheets are isolated from each other and the situation is the same as in a single F sheet, thus reducing the results of the single sheet case.

A bulk ferromagnet is represented by taking the atomic limit of the sheet separation ($d \to a$), in which $\Gamma \to \Gamma_{\text{bulk}} = \hbar/(SJ_{sd}\tau_{\text{sf}})$, so that the z-component of the pumped spin accumulation and the additional Gilbert damping due to the s-d interaction becomes

$$\delta m_z = -\mu_{\text{B}} N(0) \frac{\hbar\omega\left(\hat{M}_+\hat{M}_-\right)}{1 + [\hbar/(SJ_{sd}\tau_{\text{sf}})]^2}, \tag{34}$$

$$\alpha_{\text{SP}} = \frac{\hbar\gamma}{4\pi M_s\lambda_s} \frac{g_{\text{N}}^s}{1 + [\hbar/(SJ_{sd}\tau_{\text{sf}})]^2} \approx \frac{\hbar\mu_{\text{B}}N(0)}{M_s\tau_{\text{sf}}} \approx \frac{3}{8S}\frac{\hbar}{\varepsilon_{\text{F}}\tau_{\text{sf}}}, \tag{35}$$

where $g_{\text{N}}^s = (h/2e^2)/(\rho_{\text{N}}\lambda_s)$. The parameter values of $N(0) = 10^{23}\,\text{eV}^{-1}\,\text{cm}^{-3}$, $\tau_{\text{sf}} = 10^{-12}$ s, and $M_s = 10^3$ Oe give $\alpha_{\text{SP}} \approx 6 \times 10^{-4}$, which is much smaller than the typical damping parameter of order of 10^{-2} in transition metal ferromagnets (Co, Fe, Ni, and their alloys) [39].

Spin Pumping from Two Ferromagnetic Sheets

It has been shown that the resonant line width in ferromagnetic layers separated by normal-metal spacers is dramatically narrowed when the resonance fields of the F

layers approached each other [45]. Here, the two ferromagnetic sheets in a normal metal shown in Fig. 1b are considered to investigate how the spin pumping is modified in the presence of two sheets, particularly the dependence of pumped spin accumulation on their sheet separation and relative precessional motion.

The magnetizations of the two F sheets are represented by the two-dimensional δ-function at $x = x_1$ and $x = x_2$,

$$\mathbf{M}(x,t) = \mathbf{M}_1(t)\delta(x - x_1) + \mathbf{M}_2(t)\delta(x - x_2). \tag{36}$$

The coupled equations of the LLG equation for $\mathbf{M}_i(t)$ ($i = 1, 2$) and the Bloch equation for $\delta\mathbf{m}(x, t)$ are

$$\frac{\partial}{\partial t}\mathbf{M}_i = -\gamma\mathbf{M}_i \times \left[\mathbf{H} + \mathbf{h}_{ac}^i(t) + J_{\text{ex}}\mathbf{m}(x_i,t)\right] + \alpha_0\hat{\mathbf{M}}_i \times \frac{\partial\mathbf{M}_i}{\partial t}, \tag{37}$$

$$\delta\mathbf{m}(x,t) = \frac{1}{\Gamma_a}\sum_{j=1}^{2}\left[\hat{\mathbf{M}}_j \times \delta\mathbf{m}\left(x_j,t\right) - \frac{\chi_e}{\gamma_e}\frac{\partial\hat{\mathbf{M}}_j}{\partial t}\right] e^{-|x-x_j|/\lambda_s}, \tag{38}$$

where $\mathrm{h}_{ac}^i(t)$ is a microwave field applied on $\mathbf{M}_i(t)$. Making the dot and cross products of $\hat{\mathbf{M}}_i(t)$ and Eq. 38 at $x = x_j$, one has the coupled equations for $\hat{\mathbf{M}}_i(t) \cdot \delta\mathbf{m}(x_j, t)$ and $\hat{\mathbf{M}}_i(t) \times \delta\mathbf{m}(x_j, t)$, the solutions of which are used in Eq. 38 to derive $\delta\mathbf{m}(x, t)$ as a function of $\mathbf{M}_1(t)$ and $\mathbf{M}_2(t)$. Using the calculated $\delta\mathbf{m}(x, t)$ in Eq. 37, the effective LLG equations are obtained for $\mathbf{M}_1(t)$ and $\mathbf{M}_2(t)$.

It is interesting to consider the situation where applied microwave fields, $\mathbf{h}_{ac}^1(t)$ and $\mathbf{h}_{ac}^2(t)$, oscillate either in the same phase or in the π phase difference. The corresponding magnetization precessions driven by the microwaves are the in-phase oscillation mode ($\mathbf{M}_1 = \mathbf{M}_2$) and the out-of-phase oscillation mode $\left(M_1^{x,y} = -M_2^{x,y}, M_1^z = M_2^z\right)$ as shown in Fig. 2a, b.

In the *in-phase* mode in Fig. 2a, the z-component of pumped spin accumulation is time independent and given by

$$\delta m_z(x) = -\frac{\mu_{\text{B}}N(0)}{1+\Gamma_+^2}\hbar\omega\left(\hat{M}_+\hat{M}_-\right)\frac{e^{-|x-x_1|/\lambda_s} + e^{-|x-x_2|/\lambda_s}}{1+e^{-d/\lambda_s}}, \tag{39}$$

where $d = |x_2 - x_1|$ is the distance between the two sheets and

$$\Gamma_+ = \frac{\Gamma_a}{1+e^{-d/\lambda_s}}, \tag{40}$$

where Γ_a is given in Eq. 15.

In the *out-of-phase* mode in Fig. 2b, the z-component of pumped spin accumulation is [46]

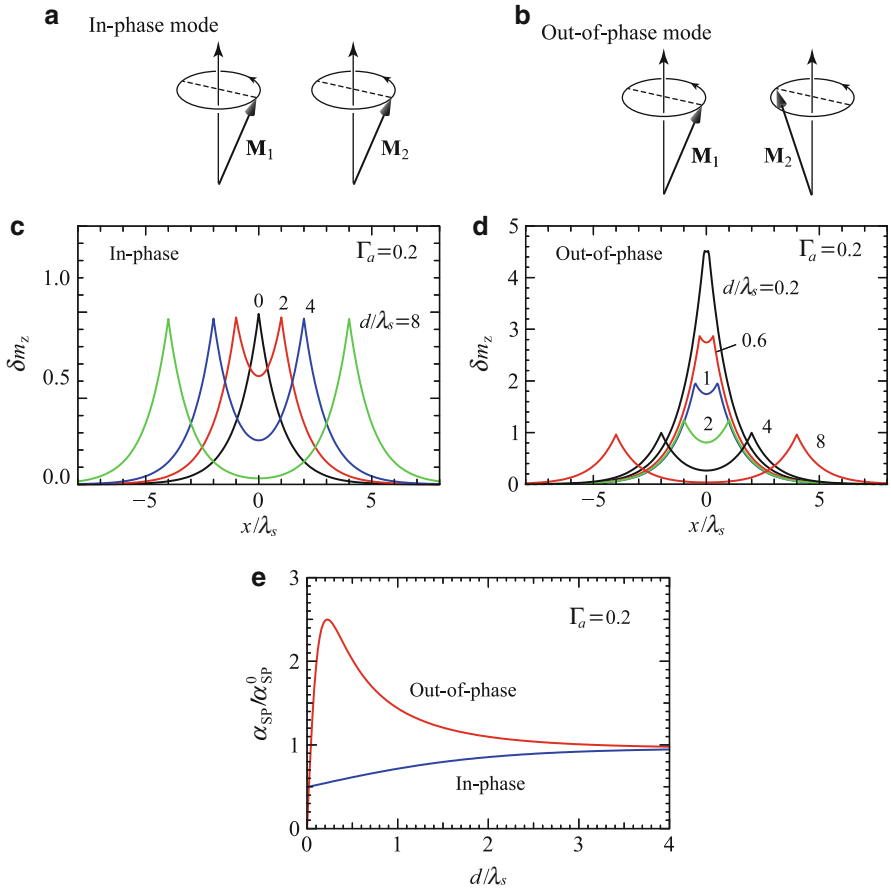

Fig. 2 (**a**) In-phase mode and (**b**) out-of-phase mode of two precessing magnetizations $\mathbf{M}_1(t)$ and $\mathbf{M}_2(t)$. Spatial variation of pumped spin accumulation in the in-phase mode (**c**) and out-of-phase mode (**d**) of the magnetizations at $x = \pm d/2$ for $\Gamma_a = 0.2$ and different sheet separation d. (**e**) Additional Gilbert damping parameter $\alpha_{\rm SP}$ as a function of sheet separation d

$$\delta m_z(x) = -\frac{\mu_{\rm B} N(0)}{1+\Gamma_-^2}\hbar\omega\left(\hat{M}_+\hat{M}_-\right)\frac{e^{-|x-x_1|/\lambda_s}+e^{-|x-x_2|/\lambda_s}}{1-e^{-d/\lambda_s}}, \tag{41}$$

where

$$\Gamma_- = \frac{\Gamma_a}{1-e^{-d/\lambda_s}}, \tag{42}$$

which indicates that Γ_- becomes larger than Γ_a when the distance d becomes smaller than the spin-diffusion length λ_s.

The effective LLG equation for the magnetizations has the same form as Eq. 16 with the renormalized parameters,

$$\alpha_{\pm} = \frac{\widetilde{\gamma}_{\pm}}{\gamma}\left(\alpha_0 + \alpha_{\rm SP}^{\pm}\right), \quad \widetilde{\gamma}_{\pm} = \frac{\gamma}{1 + \alpha_{\rm SP}^{\pm}/\Gamma_{\pm}}, \tag{43}$$

where the subscript + (−) denotes the quantities for the in-phase (out-of-phase) mode and $\alpha_{\rm SP}^{\pm}$ is the additional Gilbert damping constant due to spin pumping [46],

$$\alpha_{\rm SP}^{\pm} = \frac{\gamma}{\gamma_e}\chi_e J_{\rm ex}\frac{\Gamma_{\pm}}{1 + (\Gamma_{\pm})^2} = \alpha_{\rm SP}^0\frac{1 \pm e^{-d/\lambda_s}}{\left(1 \pm e^{-d/\lambda_s}\right)^2 + \Gamma_a^2}, \tag{44}$$

where $\alpha_{\rm SP}^0 = (\hbar\gamma/2\pi M_s a) g_{\rm N}^s$.

Figure 2 shows the spatial variation of spin accumulation $\delta m_z(x)$ normalized to $\mu_{\rm B}N(0)\hbar\omega(\hat{M}_+\hat{M}_-)$ and pumped by the in-phase and out-of-phase precessing magnetizations for $\Gamma_a = 0.2$ and different sheet separation d. In the in-phase mode shown in Fig. 2c, the peak hight $\delta m_z(x_i)$ is nearly independent of sheet separation because of weak d-dependence of Γ_+. By contrast, in the out-of-phase mode in Fig. 2d, a giant enhancement of spin pumping occurs for a small sheet separation, as seen in the curve of $d/\lambda_s = 0.2$, when the condition $\alpha_{\rm SP}^0 \ll \alpha_0$ is satisfied. Calculations for large $\Gamma_a(\Gamma_a > 1)$ show quite different behaviors; the spin pumping in the out-of-phase mode is strongly suppressed for smaller distance ($d < \lambda_s$) due to the destructive interlayer spin current.

Figure 2e shows the additional Gilbert damping $\alpha_{\rm SP}$ due to spin pumping in the in-phase and out-of-phase modes of the magnetizations for $\Gamma_a = 0.2$. In the out-of-phase mode, $\alpha_{\rm SP}$ increases with decreasing layer separation from $\alpha_{\rm SP}^0$ and has a peak at $L/\lambda_s = -\ln(1 - \Gamma_a) \approx \Gamma_a$ with the maximum value $\alpha_{\rm SP}^{\rm out}/\alpha_{\rm SP}^0 \sim (2\Gamma_a)^{-1} \sim 2.5$, for which the spin pumping is strongly enhanced to generate a large spin accumulation, as seen in Fig. 2d. In the in-phase mode, by contrast, $\alpha_{\rm SP}$ decreases with decreasing layer separation from $\alpha_{\rm SP}^0 (L \gg \lambda_s)$ to $\alpha_{\rm SP}^0/2 (L \ll \lambda_s)$. It is interesting to note that in the out-of-phase mode, there is an optimum layer separation at which the giant spin pumping and the enhanced Gilbert damping occurs simultaneously, whereas in the in-phase mode, the spin-pumping efficiency is rather independent of the layer separation, while the Gilbert damping decreases with decreasing the separation.

The giant spin pumping and enhanced Gilbert damping can be tested by experiments by using a thin insulating ferromagnetic layer, such as yttrium-iron-garnet (YIG), for the ferromagnetic layers, in which an ac current is applied to the central normal-metal spacer layer, thereby producing Oersted microwave fields on the adjacent magnetizations and driving them in the out-of-phase precession motion [46].

Spin Pumping from a Ferromagnetic Layer with *N* Ferromagnetic Sheets

To describe spin pumping in a realistic situation, an array of ferromagnetic sheets is introduced in a normal metal to form a ferromagnetic layer where all the spins coherently precess (in-phase) by microwave as shown in Fig. 1d. In this situation, the ferromagnetic layer is represented by the array of two-dimensional δ-functions at $x_n = na$ $(n = 1, 2, \cdots, N)$ with atomic distance a as

$$\mathbf{M}(x,t) = \mathbf{M}_a(t)\sum_{n=1}^{N}\delta(x - x_n) = \mathbf{M}(t)a\sum_{n=1}^{N}\delta(x - x_n), \tag{45}$$

with magnetization $\mathbf{M}(t) = \mathbf{M}_a(t)/a$ and thickness $d_{\mathrm{F}} = Nd$ of the F layer. The system corresponds to a N/F/N system. Note that if the N/F/N is divided into two parts at the middle of the F layer, each of which corresponds to an F/N system with half the thickness of F ($d_{\mathrm{F}}/2$). In the present model, it is implicitly assumed that the electron transport across the interface is transparent, and the spin-diffusion length is common in the F and N layers.

In integrating the Bloch equation for spin accumulation,

$$\delta\mathbf{m}(x,t) = -\frac{1}{\Gamma_a}\sum_{j=1}^{N}\left[\frac{\chi_e}{\gamma_e}\frac{\partial}{\partial t}\hat{\mathbf{M}}(t) - \hat{\mathbf{M}}(t)\times\delta\mathbf{m}\left(x_j,t\right)\right]e^{-|x-x_j|/\lambda_s}, \tag{46}$$

and taking the dot and cross products of Eq. 46 and $\hat{\mathbf{M}}(t)$, one obtains

$$\delta\mathbf{m}(x_i,t) = -\frac{\chi_e}{\gamma_e}\sum_{j}^{N}\left(\mathbf{A}^{-1}\right)_{ij}\left[\Gamma_a\frac{\partial\hat{\mathbf{M}}}{\partial t}Y_j + \hat{\mathbf{M}}\times\frac{\partial\hat{\mathbf{M}}}{\partial t}Z_j\right], \tag{47}$$

where $\mathbf{A}^{-1}$ is the inverse matrix of $\mathbf{A}$ whose components are

$$\mathbf{A}_{ij} = \Gamma_a^2\delta_{ij} + \sum_{k=1}^{N}X_{ik}X_{kj}, \tag{48}$$

and

$$X_{ij} = e^{-|x_i-x_j|/\lambda_s}, \quad Y_j = \sum_{k=1}^{N}X_{jk}, \quad Z_j = \sum_{k=1}^{N}X_{jk}Y_k. \tag{49}$$

The LLG equation for the magnetization is written as

$$\frac{\partial}{\partial t}\hat{\mathbf{M}} = -\gamma\hat{\mathbf{M}}\times\left(\mathbf{H}_{\mathrm{eff}} + \mathbf{h}_{ac}\right) - \gamma J_{\mathrm{ex}}\hat{\mathbf{M}}\times\delta\overline{\mathbf{m}}_{\mathrm{F}} + \alpha_0\hat{\mathbf{M}}\times\frac{\partial}{\partial t}\hat{\mathbf{M}}, \tag{50}$$

where the average spin accumulation

$$\delta\overline{\mathrm{m}}_{\mathrm{F}}(t) = \frac{1}{N}\sum_{i=1}^{N} \mathrm{m}(x_i, t),$$

acts as the exchange torque on $\mathbf{M}(t)$. Using Eq. 47, the effective LLG equation of the F layer becomes

$$\frac{\partial \mathbf{M}(t)}{\partial t} = -\widetilde{\gamma}\mathbf{M}(t) \times [\mathbf{H}_{\mathrm{eff}} + \mathbf{h}_{ac}(t)] + \frac{\alpha}{M_s}\left(\mathbf{M}(t) \times \frac{\partial \mathbf{M}(t)}{\partial t}\right), \tag{51}$$

where α and $\widetilde{\gamma}$ are the renormalized Gilbert damping parameter and gyromagnetic ratio

$$\alpha = \frac{\widetilde{\gamma}}{\gamma}(\alpha_0 + \alpha_{\mathrm{SP}}), \tag{52}$$

$$\alpha_{\mathrm{SP}} = \frac{\gamma}{\gamma_e}\chi_e J_{\mathrm{ex}} \Gamma_a \frac{1}{N}\sum_{ij=1}^{N} \left(\mathbf{A}^{-1}\right)_{ij} Y_j, \tag{53}$$

$$\frac{\gamma}{\widetilde{\gamma}} = 1 + \frac{\gamma}{\gamma_e}\chi_e J_{\mathrm{ex}} \Gamma_a \frac{1}{N}\sum_{ij=1}^{N} \left(\mathbf{A}^{-1}\right)_{ij} Z_j, \tag{54}$$

which reduce the results of the preceding sections in the case of $N = 1$ and $N = 2$.

Equation 47 is numerically solved with respect to $\delta\mathbf{m}(x_j, t)$, which is used to calculate $\delta\mathbf{m}(x, t)$ in Eq. 46. The spatial variations of spin accumulation $\delta\mathbf{m}_z(x)$ and spin current $j_{sx}^z(x)$ are shown in Fig. 3a,b, respectively, for the thickness $d_{\mathrm{F}}/\lambda_s = 2$ ($N = 100$, $a/\lambda_s = 0.02$) and various values of Γ_a. In the case of small Γ_a, spins are uniformly accumulated inside the ferromagnetic region between the vertical dashed lines indicated in the figure and the spin current vanishes there and are efficiently pumped out of F into the metallic region with the large amplitude decaying exponentially in the spin-diffusion length. As Γ_a increases, the spin accumulation in F decreases near the boundaries, and the spin-pumping efficiency is reduced. As clearly seen in Fig. 3b, the length scale in the spatial variation of the spin current in F depends strongly on Γ_a, indicating that there is no definite length scale for spin accumulation in F in the case of spin pumping.

If the spin accumulation inside the F layer is approximated as a constant and denoted by $\delta\mathbf{m}_{\mathrm{F}}(t)$, the analytical expression is obtained as

$$\delta\mathbf{m}_{\mathrm{F}}(t) = -\frac{\chi_e}{\gamma_e}\frac{\Gamma_N}{1+\Gamma_N^2}\left(\frac{\partial \hat{\mathbf{M}}}{\partial t}\right) - \frac{\chi_e}{\gamma_e}\frac{1}{1+\Gamma_N^2}\left(\hat{\mathbf{M}} \times \frac{\partial \hat{\mathbf{M}}}{\partial t}\right), \tag{55}$$

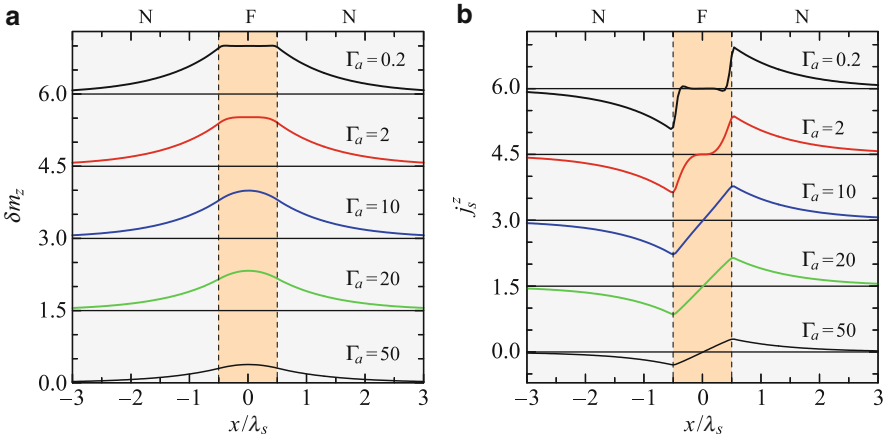

Fig. 3 Spatial variation of (**a**) pumped spin accumulation $\delta\mathbf{m}_z(x)$ normalized to $(\chi_e/\gamma_e)\omega(M_+M_-)/M_s^2$ and (**b**) pumped spin current $j_{sx}^z(x)$ for the thickness $d_F/\lambda_s = 2$ of a ferromagnetic layer with $N = 100$ sheets and different values of Γ_a in a N/F/N system. The ferromagnetic region lies between the *vertical dashed lines* and the outsides are the normal metallic region

where

$$\Gamma_N = \frac{\Gamma_a}{\left(\sum_j Y_j^2/N\right)^{1/2}} \approx \frac{\Gamma_a}{\sum_j Y_j/N} \approx \frac{\Gamma_{\rm bulk}}{1-(1-e^{-d_F/\lambda_e})/(d_F/\lambda_s)}, \tag{56}$$

indicating that Γ_N varies as $\Gamma_N \approx (2\lambda_s/d_F)\Gamma_{\rm bulk}$ for $d_F < \lambda_s$ and tends to the bulk value $\Gamma_{\rm bulk} = (a/2\lambda_s)\Gamma_a = \hbar/(SJ_{sd}\tau_{sf})$ for $d_F \gg \lambda_s$. In this approximation, the renormalized parameters in Eqs. 52, 53, and 54 become

$$\alpha = \frac{\widetilde{\gamma}}{\gamma}(\alpha_0 + \alpha_{\rm SP}), \tag{57}$$

$$\alpha_{\rm SP} = \frac{\gamma}{\gamma_e}\chi_e J_{\rm ex}\frac{\Gamma_N}{1+\Gamma_N^2}, \tag{58}$$

$$\frac{\gamma}{\widetilde{\gamma}} = 1 + \frac{\gamma}{\gamma_e}\chi_e J_{\rm ex}\frac{1}{1+\Gamma_N^2}. \tag{59}$$

For the parameter values of $d_N/\lambda_s = 2$ and $a/\lambda_s = 0.02$ in Fig. 3, $\Gamma_N \approx 0.02\Gamma_a$.

Figure 4a shows the additional Gilbert damping parameter $\alpha_{\rm SP}$ as a function of thickness d_F for $a/\lambda_s = 0.02$ and different values of Γ_a. The numerical results are well reproduced by the analytical calculation. It follows from Eq. 58 that $\alpha_{\rm SP}$ has a peak at $\Gamma_N = 1$, which corresponds to the layer thickness $d_F/\lambda_s \approx (a/\lambda_s)\Gamma_a$ if $d_F \ll \lambda_s$, e.g., $d_F/\lambda_s \approx 0.2$ in the case of $\Gamma_a = 10$, as seen in Fig. 4a. On the other hand, in the case of small Γ_a, $\alpha_{\rm SP}$ decreases linearly with increasing thickness d_F in a wide

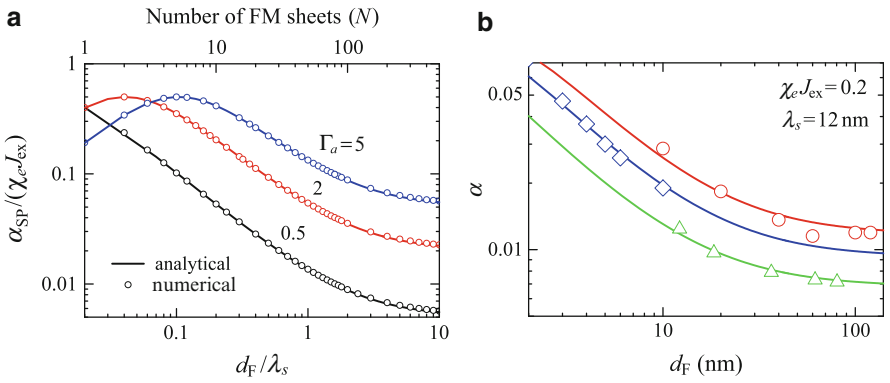

Fig. 4 (**a**) Additional Gilbert damping parameter α_{SP} as a function of thickness d_F for $\Gamma_a = 0.5$, 2, 10. The *open circles* and *solid curves* are the results of numerical calculation and analytical approximation, respectively. (**b**) Gilbert damping parameter α as a function of thickness d_F. The *diamonds* are the experimental values for trilayer Pt/Py/Pt systems ($d_F = d_{Py}$) by Mizukami et al. [47], and the *triangles* and *circles* are those for bilayer Py/Pt systems ($d_F = 2d_{Py}$) by Azevedo et al. [48] and Nakayama et al. [49], respectively. The *solid lines* are fitting by the present model

range, as seen in the curve of $\Gamma_a = 0.5$. In this range, Eq. 56 becomes $\Gamma_N = (a/d_F)\Gamma_a = 2(\lambda_s/d_F)\Gamma_{bulk}$, so that

$$\alpha_{SP} \approx \frac{\hbar\gamma}{2\pi M_s d_F} \frac{h}{2e^2} \frac{1}{\rho_N \lambda_s}, \tag{60}$$

indicating that the additional Gilbert damping due to spin pumping is inversely proportional to the F thickness [14]. In the thick case ($d_F \gg \lambda_s$), $\Gamma_N = (a/\lambda_s)\Gamma_a$ and α_{SP} tend to a constant value.

Figure 4b shows the thickness dependence of the experimental Gilbert damping α measured in Py/Pt systems by FMR [47–49]. The solid curves represent the theoretical fit using Eqs. 56, 57, and 58 with the parameter values $\chi_e J_{ex} = 0.2$ and $\lambda_s = 12$ nm, and $(\Gamma_{bulk}, \alpha_0) = (0.041, 0.0055)$ for the top curve, (0.03, 0.005) for the middle curve, and (0.017, 0.0045) for the bottom curve, where $\gamma = \gamma_e$ is assumed.

According to the theory of spin pumping based on the scattering formalism [14, 33, 32], the additional Gilbert damping constant is given by

$$\alpha_{SP} = \frac{1}{2\pi} \frac{\hbar\gamma}{M_s d_F} \frac{g_{\uparrow\downarrow}}{1 + \left(g_{\uparrow\downarrow}/g_N^s\right)}, \quad (d_N \gg \lambda_s), \tag{61}$$

where $g_{\uparrow\downarrow}$ is the so-called spin mixing conductance and $g_N^s = (h/2e^2)/(\rho_N \lambda_s)$. In the case of transparent interface $\left(g_{\uparrow\downarrow} \gg g_N^s\right)$, Eq. 61 reduces exactly to Eq. 60. This transparent condition requires $g_{\uparrow\downarrow} \gg g_N^s = 10^{15}\text{cm}^{-2}$ for a metal with $\rho_N \sim 20\ \mu\Omega$ cm and $\lambda_s \sim 10$ nm like Pt or Pd. Recent experiments indicate that the mixing conductance has large values up to $g_{\uparrow\downarrow} \sim 10^{16}\ \text{cm}^{-2}$ for various ferromagnets [50].

Spin Pumping from Ferromagnetic Insulator

Magnetic insulators, such as yttrium-iron-garnet (YIG), are useful energy-saving materials for spintronics because of their low magnetic damping and losses owing to purely magnetic excitations and almost frozen electric excitation. In the following, it is shown that the spin pumping is possible from a ferromagnetic insulator (FI) into an adjacent normal metal (N) in a bilayer system such as YIG/Pt, which originates from the spin-exchange interaction between a conduction electron in Pt and a localized moment in YIG at the interface [51, 52]. The effect of exchange interaction is incorporated in the Landau-Lifshitz-Gilbert (LLG) equation for the magnetization of FI and the diffusion-modified Bloch equation for spin accumulation in N [53], which is solved to derive the spin current pumped from FI into N. By combining the pumped spin current with the inverse spin-Hall effect (ISHE) [21], one obtains the output voltage V appeared between the N ends as a function of the exchange coupling.

At the FI/N interface, conduction electrons in N interact with magnetic moments of FI through the so-called s-d exchange interaction [41],

$$H_{\mathrm{sd}} = -J_{sd} v_a \sum_{i \in \mathrm{I}} \hat{\mathbf{S}}_i(t) \cdot \hat{\mathbf{s}}(\mathbf{r}_i, t), \tag{62}$$

where $\hat{\mathbf{s}}(\mathbf{r}_i, t)$ and $\hat{\mathbf{S}}_i(t)$ are the conduction-electron spin density and the localized spin at lattice site i on the interface (I) at $x = 0$ and J_{sd} is the exchange coupling strength between them. When the aligned localized spins are uniformly precessed by a microwave field, $\hat{\mathbf{S}}_i$ can be replaced by the magnetization $\mathbf{M}$ using the relation $\hat{\mathbf{S}}_i(t)/S = -\mathbf{M}(t)/M_s$ [39], which enables to rewrite Eq. 62 as

$$H_{\mathrm{sd}} = -J_{\mathrm{ex}} \int dx \mathbf{M}(t) a_S \delta(x) \cdot \mathbf{m}(x, t), \tag{63}$$

where $J_{\mathrm{ex}} = v_a J_{sd}/(\hbar^2 \gamma \gamma_e) = (v_a/v_S) J_{sd} S/(\hbar \gamma_e M_s)$ is the dimensionless exchange coupling constant, S is an effective block spin per unit cell, γ_e is the gyromagnetic ratio of conduction electron, $a_S(a)$ is the lattice constant, $v_S = a_S^3 (v_a = a^3)$ is the unit cell volume for localized moment (conduction electron), and $\mathbf{m}(x, t)$ is the magnetization of conduction electrons. Equation 63 indicates that $\mathbf{M}(t) a_S \delta(x)$ plays a role of the interface magnetization and gives rise to the mutually exerted spin torque on $\mathbf{M}$ and $\mathbf{m}$ as follows:

$$[d\mathbf{m}(x, t)/dt]_{\mathrm{ex}} = -[d\mathbf{M}(t)/dt]_{\mathrm{ex}} = -\gamma_e J_{\mathrm{ex}} \mathbf{m}(x, t) \times \mathbf{M}(t) a_S \delta(x) \tag{64}$$

through the exchange interaction at the interface.

By including the exchange spin torque in the LLG equation and integrating with respect to x,

$$\frac{\partial}{\partial t}\mathbf{M}(t) = -\gamma \mathbf{M}(t) \times [\mathbf{H}_{\text{eff}} + \mathbf{h}_{ac}(t)] - \frac{a_S}{d_F}\gamma J_{\text{ex}}[\mathbf{M}(t) \times \mathbf{m}(0,t)] + \alpha_0 \hat{\mathbf{M}}(t) \times \frac{\partial}{\partial t}\mathbf{M}(t), \tag{65}$$

where $\mathbf{h}_{ac}(t)$ is the microwave field, γ is the gyromagnetic ratio of FI, and α_0 is the Gilbert damping constant of FI. The magnetization of conduction electrons is written as $\mathbf{m}(x, t) = \mathbf{m}_0(t)a_S\delta(x) + \delta\mathbf{m}(x, t)$, where $\mathbf{m}_0(t) = \chi_e J_{\text{ex}}\mathbf{M}(t)$ is the local equilibrium spin density, $\chi_e = 2\mu_B^2 N(0)$ is the spin susceptibility of conduction electrons, and $\delta\mathbf{m}(x, t)$ is spin accumulation.

The Bloch equation with the exchange spin torque and the spin diffusion is given by

$$\frac{\partial}{\partial t}\mathbf{m}(x,t) = -\gamma_e J_{\text{ex}}[\mathbf{m}(x,t) \times \mathbf{M}(t)]a_S\delta(x) - \frac{\delta\mathbf{m}(x,t)}{\tau_{\text{sf}}} + D\nabla^2\delta\mathbf{m}(x,t), \tag{66}$$

where τ_{sf} is the spin-flip relaxation time and D is the diffusion constant. With the precession frequency (~GHz) much smaller than the spin-flip relaxation rate $\left(\tau_{\text{sf}}^{-1} \sim 10^{12}\text{s}^{-1}\right)$, the solutions of Eq. 66 are obtained for the transverse spin accumulation $\delta m_{\pm} = \delta m_x \pm i\delta m_y$, which are used to calculate the longitudinal spin accumulation

$$\delta m_z(x) = \frac{1}{\Gamma_s M_s}\text{Im}[\delta m_+(0,t)M_-(t)]e^{-x/\lambda_s}, \quad (x > 0) \tag{67}$$

where

$$\Gamma_s = \frac{\hbar}{SJ_{sd}\tau_{\text{sf}}}\frac{\lambda_s}{a_{\text{eff}}} \tag{68}$$

and $M_{\pm}(t) = M_x(t) \pm iM_y(t)$, $\lambda_s = \sqrt{D\tau_{\text{sf}}}$ is the spin-diffusion length, and $a_{\text{eff}} = (a/a_S)^3 a_S$. Note that the factor $(\lambda_s/a_{\text{eff}})$ appears in Γ_s due to the exchange interaction restricted to the interface with the effective exchange interaction range a_{eff}.

The calculated spin accumulations are expressed in the vector form

$$\delta\mathbf{m}(x,t) = -\frac{\chi_e}{\gamma_e}\left[\frac{1}{1+\Gamma_s^2}\left(\hat{\mathbf{M}} \times \frac{\partial\hat{\mathbf{M}}}{\partial t}\right) + \frac{\Gamma_s}{1+\Gamma_s^2}\left(\frac{\partial\hat{\mathbf{M}}}{\partial t}\right)\right]e^{-x/\lambda_s}, \tag{69}$$

which is used in Eq. 69 to yield the effective LLG equation

$$\frac{\partial\mathbf{M}}{\partial t} = -\widetilde{\gamma}\,\mathbf{M} \times (\mathbf{H}_{\text{eff}} + \mathbf{h}_{ac}) + \frac{\alpha}{M_s}\left(\mathbf{M} \times \frac{\partial\mathbf{M}}{\partial t}\right), \tag{70}$$

with the renormalized Gilbert damping constant and gyromagnetic ratio

$$\alpha = \frac{\widetilde{\gamma}}{\gamma}(\alpha_0 + \alpha_{\rm SP}), \quad \widetilde{\gamma} = \frac{\gamma}{1 + (\alpha_{\rm SP}/\Gamma_s)}, \tag{71}$$

where

$$\alpha_{\rm SP} = \frac{a_{\rm eff}}{d_{\rm F}} \frac{\gamma}{\gamma_e} \chi_e J_{\rm ex} \frac{\Gamma_s}{1+\Gamma_s^2} = \frac{1}{4\pi} \frac{\hbar\gamma}{M_s d_{\rm F}} \frac{g_{\rm N}^s}{1+\Gamma_s^2}, \quad g_{\rm N}^s = \frac{h}{2e^2\rho_{\rm N}\lambda_s}, \tag{72}$$

and $\rho_{\rm N}$ is the electrical resistivity of the normal metal.

The pumped spin current is given by $\mathbf{j}_{sx} = \gamma_e^{-1} D \nabla_x \delta\mathbf{m}$, whose z-component is

$$j_{sx}^z = \frac{\hbar\omega}{8\pi} \frac{g_{\rm N}^s}{1+\Gamma_s^2} \left(\frac{M_+ M_-}{M_s^2}\right) e^{-x/\lambda_s}, \tag{73}$$

where $\omega = 2\pi f$ (f is a microwave frequency). Thus, the spin current strongly depends on the magnitude of the exchange coupling through Γ_s. For the strong coupling limit $\left(\Gamma_s^2 \ll 1\right)$, the spin current is independent of the exchange coupling. For the weak coupling limit $\left(\Gamma_s^2 \gg 1\right)$, the spin current is proportional to the square of the exchange coupling. In ordinary ferromagnets $\hbar/(SJ_{sd}\tau_{\rm sf}) \ll 1$, whereas $(\lambda_s/a_{\rm eff}) \gg 1$ due to the interface effect. In strong ferromagnets like Fe, Co, Ni, Py, etc., the condition $\Gamma_s^2 \ll 1$ is safely satisfied, indicating a maximum efficiency for spin pumping.

By taking into account the boundary condition that the spin current vanishes at the outer surface of N, $j_{sx}^z(x = d_{\rm N}) = 0$, the pumped spin current is expressed as

$$j_{sx}^z = \frac{\hbar\omega}{8\pi} g_{\rm N}^2 \frac{\sinh[(d_{\rm N}-x)/\lambda_s]}{\sinh(d_{\rm N}/\lambda_s)} \frac{\tanh(d_{\rm N}/\lambda_s)}{1+\Gamma_s^2\tanh^2(d_{\rm N}/\lambda_s)} \left(\frac{M_+ M_-}{M_s^2}\right), \tag{74}$$

which gives rise to the electric field E along the y direction by the inverse spin-Hall effect (ISHE): $\sigma_{\rm N} E = \theta_{\rm SHE}(2e/\hbar)\left\langle j_{sx}^z(x)\right\rangle_x$, where $\langle\cdots\rangle_x$ is the average over x. Thus, the output voltage $V = w_{\rm N}E$ between the Pt ends with length $w_{\rm N}$ is given by

$$V \approx \theta_{\rm SH} \frac{\hbar\omega}{4e} \left(\frac{w_{\rm N}}{d_{\rm N}}\right) \left(\frac{\gamma h_{ac}}{\alpha\omega}\right)^2 \frac{\tanh(d_{\rm N}/\lambda_s)\tanh(d_{\rm N}/2\lambda_s)}{1+\Gamma_s^2\tanh^2(d_{\rm N}/\lambda_s)}, \tag{75}$$

at the resonance condition $(\omega = \widetilde{\gamma}H)$. Equation 75 enables one to estimate the magnitude of the exchange interaction J_{sd} from a measured value of voltage V at resonance.

Using the measured value $V = 4.8\ \mu$V by Kajiwara et al. [52] together with experimental parameters, $d_{\rm N} = 10$ nm, $w_{\rm N} = 3$ mm, $\lambda_s = 7$ nm, $\theta_{\rm SH} = 0.0037$, $\gamma = 1.76 \times 10^7\ {\rm Oe}^{-1}\ {\rm s}^{-1}$, $\alpha = 6.7 \times 10^{-5}$, $\omega = 59 \times 10^9\ {\rm s}^{-1}$, $h_{ac} = 0.11$ Oe, and $(\gamma h_{ac}/\alpha\omega) = 0.49$, one has $\Gamma_s \approx 19$. Using this Γ_s value, $\tau_{\rm sf} = 0.3$ ps, $\rho_{\rm N} = 30\ \mu\Omega$cm, $4\pi M_s$

$= 1{,}956$ Oe, $a = 0.2$ nm, $a_S = 1.24$ nm, and $S = M_s a_S^3/(\hbar\gamma) = 16$ in Eq. 68, one obtains $SJ_{sd} \sim 0.16$ eV, which is one order of magnitude smaller than those of typical ferromagnets ($SJ_{sd} \sim 1$ eV for Co, Fe, Ni, and their alloys).

According to the spin-pumping theory based on the scattering formalism [14, 33, 32], one obtains the output voltage at resonance,

$$V = \theta_{\rm SH}\frac{\hbar\omega}{4e}\left(\frac{w_{\rm N}}{d_{\rm N}}\right)\left(\frac{\gamma h_{ac}}{\alpha\omega}\right)^2 \frac{\tanh(d_{\rm N}/\lambda_s)\tanh(d_{\rm N}/2\lambda_s)}{1+\left(g_{\rm N}^s/g_{\uparrow\downarrow}\right)\tanh(d_{\rm N}/\lambda_s)}, \tag{76}$$

where $g_{\rm N}^2 = (h/2e^2)/(\rho_{\rm N}\lambda_s)$. When the mixing conductance is large, $\left(g_{\rm N}^s/g_{\uparrow\downarrow} \ll 1\right)$, which corresponds to the strong exchange interaction ($\Gamma_s \ll 1$), Eqs. 75 and 76 tend to the same result,

$$V = \theta_{\rm SH}\frac{\hbar\omega}{4e}\left(\frac{w_{\rm N}}{d_{\rm N}}\right)\left(\frac{\gamma h_{ac}}{\alpha\omega}\right)^2\left[1-\frac{1}{\cosh(d_{\rm N}/\lambda_s)}\right], \tag{77}$$

which is the highest spin-pumping efficiency. In the opposite limit, i.e., $\left(g_{\rm N}^s/g_{\uparrow\downarrow}\right) \gg 1 (\Gamma_s \gg 1)$, one has the relation $g_{\uparrow\downarrow} \sim g_{\rm N}^s/\Gamma_s^2$. The values $\Gamma_s = 19$ [52] and $g_{\rm N}^s = 6 \times 10^{14}\text{cm}^{-2}$ estimated above yield the mixing conductance $g_{\uparrow\downarrow} \approx 2 \times 10^{12}$ cm^{-2} at the interface of Pt/YIG.

Recent experiments have reported large spin mixing conductance of the order of $g_{\uparrow\downarrow} \sim 10^{13}$ cm^{-2} [54] and $\sim 10^{15}$ cm^{-2} [55] in the YIG/Pt interfaces and $g_{\uparrow\downarrow} \sim 10^{14}$–$10^{15}$ cm^{-2} in the YIG/Ag interface [56, 57], probably due to improvement of interface conditions. These results indicate that a high spin-pumping efficiency is achieved even in the FI/N system.

Manipulation of Magnetization Dynamics by Spin-Hall Effect

In the preceding section "Spin Pumping by Precessing Magnetizations," it is demonstrated that the magnetization damping of a ferromagnetic layer is enhanced by spin pumping into an adjacent normal-metal layer. The inverse effect that the magnetization dynamics is manipulated by injecting spin current from a normal-metal layer into a ferromagnetic layer is possible by using the spin-Hall effect in a normal-metal layer. The control of magnetization damping and magnetization switching has been demonstrated by experiments using materials with large spin-orbit interactions such as Pt [58–60] and Ta [61].

A simple and useful system is a bilayer film consisting of a ferromagnetic layer (F) and a normal-metal layer (N) shown in Fig. 5a, in which the external magnetic field $\mathbf{H}$ is along $\hat{\mathbf{z}}$, the applied current $\mathbf{J}$ is along $\hat{\mathbf{y}}$, and $\hat{\mathbf{x}}$ is normal to the interface. The dynamics of magnetization $\mathbf{M}$ in a F/N bilayer film is described by a generalized Landau-Lifshitz-Gilbert (LLG) equation [12, 13] including the spin torque

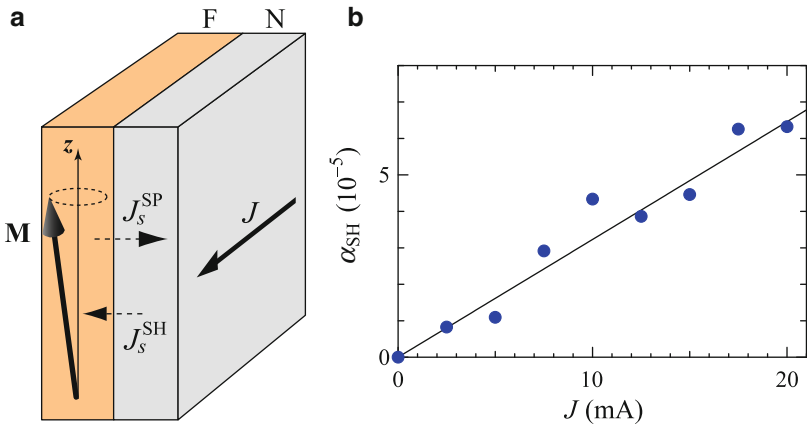

Fig. 5 (**a**) Schematic diagram of F/N bilayer system. **M** and **J** represent the magnetization and the applied electric current, respectively, and J_s^{SP} and J_s^{SH} the interface spin-current densities polarized along z due to spin pumping and SHE, respectively. (**b**) Modulation of the Gilbert damping constant $\alpha_{SH} = [\alpha(J) - \alpha(-J)]/2$ as a function of J. The *solid circles* are the experimental values for Py/Pt by Ando et al. [58]

terms due to spin pumping (SP) and spin-Hall effect (SHE). In the absence of the applied current ($\mathbf{J} = 0$), only the spin pumping from the precessing magnetization into the Pt layer contributes to a relaxation of the precessional motion and yields an additional Gilbert damping constant α_{SP}^{SP} to the intrinsic damping constant α_{Py} of an isolated Py layer [13, 33], the sum of which is denoted as $\alpha_0 = \alpha_{Py} + \alpha_{SP}$, where α_{SP} is a positive value because the spin current is pumped out of F.

In the presence of the applied current ($\mathbf{J} \neq 0$), SHE contributes to a further relaxation of the precessing magnetization and modifies the relaxation by changing the magnitude and polarity of **J** as follows. The spin current density j_{sx}^{SH} generated by SHE in the N layer is injected across the F/N interface, and the transverse component of the incident spin current is absorbed to be transferred to the magnetization, exerting a spin-transferred torque on **M** [62]:

$$\left(\frac{\partial \mathbf{M}}{\partial t}\right)_{SHE} = -\left(\gamma j_s^{SH}/d_F\right)\hat{\mathbf{M}} \times \left(\hat{\mathbf{M}} \times \hat{\boldsymbol{\sigma}}\right), \tag{78}$$

where γ is the gyromagnetic ratio, $\hat{\mathbf{M}}$ is the unit vector in the direction of magnetization **M**, $\hat{\boldsymbol{\sigma}}$ is a unit vector in the polarization direction of the spin current, and d_F is the thickness of the F layer. Thus, the generalized LLG reads

$$\frac{\partial \hat{\mathbf{M}}}{\partial t} = -\gamma \hat{\mathbf{M}} \times \mathbf{H}_{eff} + \alpha_0 \hat{\mathbf{M}} \times \frac{\partial \hat{\mathbf{M}}}{\partial t} - \frac{\gamma j_s^{SH}}{M_s d_F} \hat{\mathbf{M}} \times \left(\hat{\mathbf{M}} \times \hat{\boldsymbol{\sigma}}\right), \tag{79}$$

where the effective field $\mathbf{H}_{eff} = \mathbf{H} - 4\pi M_x \hat{\mathbf{x}} + \mathbf{h}_{ac}(t)$ is the sum of in-plane applied field H, demagnetizing field $-4\pi M_x \hat{\mathbf{x}}$, M_s is the saturation magnetization of the F layer, and linear-polarized microwave field $\mathbf{h}_{ac}(t) = (0, h_{ac}e^{-i\omega t}, 0)$ with $\omega = 2\pi f$

(f is a microwave frequency). The third term in r.h.s. of Eq. 79 is the spin-transferred torque term due to SHE.

In the present setup, the precession axis along $\hat{\mathbf{z}}$ is parallel to the polarization direction $\hat{\boldsymbol{\sigma}}$ of the injected spin current ($\hat{\boldsymbol{\sigma}} \| \hat{\mathbf{z}}$), and thus the linearized LLG equation of Eq. 79 with respect to the precession amplitude is solved to yield analytical expressions for (M_x, M_y), which enables to calculate the microwave absorption $P = -\left(\omega h_{ac}^2/2\right)\mathrm{Im}\left[\chi_{yy}\right]$ with dynamic susceptibility [63]:

$$\chi_{yy} = -\frac{\gamma M_s[\gamma(H + 4\pi M_s) + i\alpha_0\omega]}{\omega^2 - \Omega_{\mathrm{K}}^2 - \left(\gamma j_s^{\mathrm{SH}}/M_s d_{\mathrm{F}}\right)^2 - 2i\alpha\omega\gamma(H + 2\pi M_s)}. \tag{80}$$

Here, $\Omega_{\mathrm{K}} = \gamma\sqrt{H(H + 4\pi M_s)}$, $\alpha = \alpha_0 + \alpha_{\mathrm{SH}}$ is the total relaxation coefficient and α_{SH} is the relaxation coefficient due to SHE [58, 59]:

$$\alpha_{\mathrm{SH}} = \frac{j_s^{\mathrm{SH}}}{M_s d_{\mathrm{F}}} \frac{1}{H_{\mathrm{FMR}} + 2\pi M_s}, \tag{81}$$

where H_{FMR} is the resonance field satisfying

$$H_{\mathrm{FMR}} + 2\pi M_s = \left[(2\pi M_s)^2 + (\omega/\gamma)^2 - \left(j_s^{\mathrm{SH}}/M_s d_{\mathrm{F}}\right)^2\right]^{1/2}. \tag{82}$$

The applied current $\mathbf{j}_{\mathrm{N}}$ in the N layer generates the spin-Hall current $\theta_{\mathrm{SH}}\hat{\mathbf{z}} \times \mathbf{j}_{\mathrm{N}}$ flowing in the direction normal to the interface and polarized along $\hat{\mathbf{z}}$, where $\theta_{\mathrm{SH}} = \sigma_{\mathrm{SH}}/\sigma_{\mathrm{N}}$ is the Hall angle, σ_{SH} is the spin-Hall conductivity, σ_{N} is the electrical conductivity of the N layer, and $\mathbf{j}_{\mathrm{N}} = [(\sigma_{\mathrm{N}} d_{\mathrm{N}})/(\sigma_{\mathrm{N}} d_{\mathrm{N}} + \sigma_{\mathrm{F}} d_{\mathrm{F}})]\mathbf{j}$ due to the shunting effect [59, 64, 65]. Incorporating the spin current generated by SHE in the drift-diffusion equations (Valet-Fert model) [66–70] and assuming the injected spin current of the form $\mathbf{j}_s^{\mathrm{SH}} = -(\hbar/2e)\left(G_{\uparrow\downarrow}/2eA_{\mathrm{J}}\right)\delta\mu(0)\hat{\mathbf{z}}$, where $G_{\uparrow\downarrow}$ is the interface spin conductance, $\delta\mu(0)\hat{\mathbf{z}}$ is the spin accumulation polarized along $\hat{\mathbf{z}}$ at the interface, and A_{J} is the junction area, the injected spin-current density at the interface turns out to be

$$j_s^{\mathrm{SH}} = \eta\theta_{\mathrm{SH}}(\hbar/2e)(J/A_{\mathrm{N}}), \tag{83}$$

where (J/A_{N}) is the applied current density, A_{N} is the cross-sectional area of the N layer, and η is the injection efficiency

$$\eta = \frac{(\rho_{\mathrm{F}}/d_{\mathrm{F}})}{(\rho_{\mathrm{F}}/d_{\mathrm{F}}) + (\rho_{\mathrm{N}}/d_{\mathrm{N}})} \frac{\left(g_{\uparrow\downarrow}/g_{\mathrm{N}}^s\right)\tanh(d_{\mathrm{N}}/2\lambda_s)}{1 + \left(g_{\uparrow\downarrow}/g_{\mathrm{N}}^s\right)\coth(d_{\mathrm{N}}/\lambda_s)}, \quad g_{\uparrow\downarrow} = \frac{hG_{\uparrow\downarrow}}{2e^2A_{\mathrm{J}}} \tag{84}$$

with the thickness d_{N} (d_{F}), the electrical resistivity ρ_{N} (ρ_{F}), and the spin-diffusion length λ_s of the N layer. For small applied current $\gamma\left|j_s^{\mathrm{SH}}\right|/(\omega M_s d_{\mathrm{F}}) \ll 1$, the additional relaxation $\alpha_{\mathrm{SH}}(J)$ due to SHE is proportional to the applied current:

$$\alpha_{\rm SH}(J) \approx \eta\theta_{\rm SH} \frac{(2e\gamma/\hbar)/(e\omega M_s d_{\rm F})}{\sqrt{1+(2\pi\gamma M_s/\omega)^2}} \frac{J}{A_{\rm N}}, \tag{85}$$

indicating that $\alpha_{\rm SH}(J)$ varies linearly with J and takes either a positive or negative value by changing the polarity of J, because spins are ejected from F or injected into F by the polarity change. The modification of the relaxation due to SHE is observable from a microwave absorption P of ferromagnetic resonance (FMR) whose spectrum versus H is written as

$$P_w \approx \frac{1}{4} h_{ac}^2 \omega \left(\frac{H_{\rm FMR}+4\pi M_s}{H_{\rm FMR}+2\pi M_s}\right) \frac{M_s(\alpha\omega/\gamma)}{(H-H_{\rm FMR})^2+(\alpha\omega/\gamma)^2}, \tag{86}$$

where $H_{\rm FMR}$ is the resonance field satisfying $\omega = \gamma\sqrt{H_{\rm FMR}(H_{\rm FMR}+4\pi M_s)}$.

The resonance width W of the FMR spectrum is given by $W = \left(2/\sqrt{3}\right)(\alpha\omega/\gamma)$, and the difference of which at $\pm J$ leads to

$$2\alpha_{\rm SH} = \alpha(J) - \alpha(-J) = \left(\sqrt{3}\gamma/2\omega\right)[W(J) - W(-J)]. \tag{87}$$

This relation allows one to obtain $\alpha_{\rm SH}$ by measuring the FMR widths of current polarities $\pm J$. Once the value of $\alpha_{\rm SH}$ is obtained by analyzing the FMR spectra, the product $\eta\theta_{\rm SH}$ is readily estimated from Eq. 85. Figure 5b shows $\alpha_{\rm SH}$ as a function of applied current J. The solid line is a fit to the experimental data by Ando et al. [58] using Eq. 85, yielding $\eta\theta_{\rm SH} \approx 0.09$ for $4\pi M_s = 6.1$ kOe, $f = 9.441$ GHz, $d_{\rm N} = d_{\rm F} =$ 10 nm, and $w_{\rm N} = 0.02$ cm. For the parameters of $\rho_{\rm N} = 15.6\,\mu\Omega$cm, $\rho_{\rm F} = 15.4\,\mu\Omega$cm, and $\lambda_s^{\rm N} = 5$ nm at room temperature, the injection efficiency is $\eta \sim 0.4$, and hence the Hall angle of the Pt layer is $\theta_{\rm SH} \sim 0.2$. The large spin-injection efficiency is promising for spintronics application utilizing SHE in manipulating the magnetization dynamics.

When the applied current is large enough and the anti-damping contribution due to SHE cancels out the intrinsic magnetization damping, the total damping coefficient vanishes at the critical current density,

$$j_{\rm cr} = -\frac{2e}{\hbar}\frac{\alpha_0}{\eta\theta_{\rm SH}} d_{\rm F} M_s (H + 2\pi M_s), \tag{88}$$

above which the magnetization switching or the spontaneous magnetization oscillation occurs by means of SHE. For $\alpha_0 = 0.01$, $\eta\theta_{\rm SH} = 0.1$, $d_{\rm F} = 20$ nm, and $M_s =$ 500 Oe, the critical current density is of the order of 10^7 A/cm^2.

Thermal Spin Pumping

Recent observation of the spin Seebeck effect [71–74] and the transmission of electrical signal through insulating ferromagnets [52, 75] have opened new possibilities in both fundamentals and applications in spintronics [30]. Ferromagnetic

insulators are unique in that they are electrically inactive with frozen charge degrees of freedom but magnetically active due to spins of localized electrons. Low-lying collective spin excitation, spin wave (magnon), carries spin angular momentum. Utilizing pure spin excitation without charge excitation is crucial for developing energy-saving spintronic devices.

In this section, it is demonstrated that the spin current flows across the interface between a ferromagnetic insulator and a normal metal in the presence of temperature difference between them. The spin-flip scattering of conduction electrons through the exchange interaction with local moments at the interface creates a magnon excitation in the ferromagnet [51]. Making use of linear-response theory and fluctuation-dissipation theorem, an analytical expression is obtained for the spin current through the interface generated by the temperature difference. The spin Seebeck effect is briefly discussed.

Spin Pumping Due to Temperature Difference

When conduction electrons in N are incident on FI, the electrons are reflected back at the FI/N interface, since electrons are prohibited to enter FI due to the large energy gap at the Fermi energy. At the scattering, there are spin-flip processes in which an electron reverses its spin from down to up or up to down, thereby emitting or absorbing a magnon in FI as shown in Fig. 6. The spin-flip scattering involving magnon excitation gives rise to transfer of spin angular momentum between FI and N. In the equilibrium situation where the temperatures of FI and N are equal, the scattering processes of (a) and (b) in Fig. 6 are balanced with each other and no spin current flows across the FI/N interface. In the nonequilibrium situation where the temperatures of FI and N are different, one of the spin-flip processes dominates over the reversed process, so that the spin current flows across the FI/N interface.

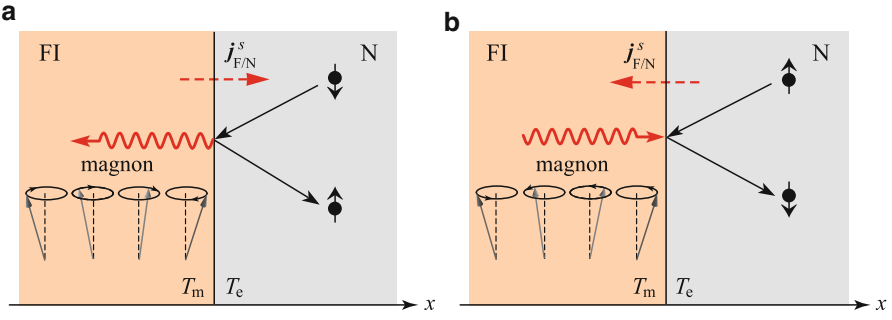

Fig. 6 Quantum mechanical spin-exchange processes at the interface of a ferromagnetic insulator (FI) and normal-metal (N) junction. (**a**) They (**b**) represent the magnon emission and absorption associated with the spin-flip scattering of conduction electrons at the interface, respectively, thereby transferring spin angular momentum $\hbar$ from FI to N and from N to FI via the exchange interaction

The electron-magnon interaction at the interface can be described by using the *s-d* exchange interaction between local moments and conduction electrons at the interface:

$$H_{\rm sd} = \frac{J_{sd}}{N_a}\sum_{n=1}^{N_{\rm I}}\int d^3r \mathbf{S}_n \cdot \psi^\dagger_{\sigma'}(\mathbf{r}_n)\hat{\boldsymbol{\sigma}}_{\sigma'\sigma}\psi_\sigma(\mathbf{r}_n), \tag{89}$$

where $\mathbf{S}_n$ are local moments at position $\mathbf{r}_n$ on the interface; $\psi^\dagger_\sigma(\mathbf{r}_n)$ and $\psi_\sigma(\mathbf{r}_n)$ are the annihilation operator of an incident electron with spin σ at position $\mathbf{r}_n$, respectively; $\hat{\boldsymbol{\sigma}}$ is the Pauli spin operator; N_a is the number of lattice sites in N; and $N_{\rm I}$ is the number of local moments that interact with conduction electrons at the interface. Using the Fourier transformation $\psi_\sigma(\mathbf{r}) = \sum_{\mathbf{k}} c_\sigma(\mathbf{k})e^{i\mathbf{k}\cdot\mathbf{r}}$ and $\mathbf{S}_n = N_S^{-1/2}\sum_{\mathbf{q}}\mathbf{S}_{\mathbf{q}}e^{i\mathbf{q}\cdot\mathbf{r}_n}$, where $c_{\mathbf{k}\sigma}$ is the annihilation operator of an incident electron with momentum $\mathbf{k}$ and spin σ and N_S is the number of localized moments in FI, Eq. 89 is written as

$$H_{sd} = J_{\rm eff}\sum_{k,k',q}\left[S^-_{\mathbf{q}}c^\dagger_{\mathbf{k}'\uparrow}c_{\mathbf{k}\downarrow} + S^+_{\mathbf{q}}c^\dagger_{\mathbf{k}'\downarrow}c_{\mathbf{k}\uparrow} + S^z_{\mathbf{q}}\left(c^\dagger_{\mathbf{k}'\uparrow}c_{\mathbf{k}\uparrow} - c^\dagger_{\mathbf{k}'\downarrow}c_{\mathbf{k}\downarrow}\right)\right]\rho_{\mathbf{q}-\mathbf{k}'+\mathbf{k}}, \tag{90}$$

where $J_{\rm eff} = J_{sd}/\left(N_a N_S^{1/2}\right)$, $S^\pm_{\mathbf{q}} = S^x_{\mathbf{q}} \pm iS^y_{\mathbf{q}}$, and $\rho_{\mathbf{p}-\mathbf{k}'+\mathbf{k}} = \sum_{n=1}^{N_{\rm I}} e^{i(\mathbf{p}-\mathbf{k}'+\mathbf{k})\cdot\mathbf{r}_n}$.

The spin current through the interface is calculated from $J^s_{\rm F/N} = (\hbar/2)(d/dt)\left(\left\langle N_e^\uparrow\right\rangle - \left\langle N_e^\downarrow\right\rangle\right)$, where $N_e^\sigma = \sum_{\mathbf{k}} c^\dagger_{\mathbf{k}\sigma}c_{\mathbf{k}\sigma}$ is the number operator of electrons with spin σ. Within the second-order perturbation with respect to J_{sd} [76], the spin current $J^s_{\rm F/N}$ across the interface is obtained as

$$\begin{aligned} J^s_{\mathbf{F/N}} = \frac{1}{\hbar}N_{\rm I}J^2_{\rm eff}\int_{-\infty}^{\infty} dt\Big[&e^{i\delta\mu t/\hbar}\left\langle S^-_{-\mathbf{q}}(t)S^+_{\mathbf{q}}(0)\right\rangle\left\langle \sigma^+_{\mathbf{q}}(t)\sigma^-_{-\mathbf{q}}(0)\right\rangle \\ &- e^{-i\delta\mu t/\hbar}\left\langle S^+_{\mathbf{q}}(t)S^-_{-\mathbf{q}}(0)\right\rangle\left\langle \sigma^+_{-\mathbf{q}}(t)\sigma^-_{\mathbf{q}}(0)\right\rangle\Big], \end{aligned} \tag{91}$$

where $\left\langle S^+_{\mathbf{q}}(t)S^-_{-\mathbf{q}}(0)\right\rangle$ and $\left\langle \sigma^+_{\mathbf{q}}(0)\sigma^-_{-\mathbf{q}}(t)\right\rangle$ are the spin correlation functions for local moments and conduction electrons, respectively; $\sigma^+_{\mathbf{p}} = \sum_{\mathbf{k}} c^\dagger_{\mathbf{k}\uparrow}c_{\mathbf{k}+\mathbf{p}\downarrow}$; and $\sigma^-_{\mathbf{p}} = \sum_{\mathbf{k}} c^\dagger_{\mathbf{k}\downarrow}c_{\mathbf{k}+\mathbf{p}\uparrow}$. Note that the spin-flip scattering of an electron at the interface produces the energy change by $\delta\mu = \mu_\uparrow - \mu_\downarrow$, which appears as the time-dependent phase factor in Eq. 91. It follows from the fluctuation-dissipation theorem [77] that the correlation functions are expressed in terms of the imaginary parts of the dynamical spin susceptibilities of F as

$$\left\langle S^-_{-\mathbf{q}}(t)S^+_{\mathbf{q}}(0)\right\rangle = -\frac{\hbar}{\pi}\int_{-\infty}^{\infty} d\omega e^{-i\omega t}n(\omega, T_\alpha){\rm Im}\chi^{+-}_\alpha(\mathbf{q},\omega), \tag{92}$$

$$\left\langle S_{\mathbf{q}}^{+}(t)S_{-\mathbf{q}}^{-}(0)\right\rangle = -\frac{\hbar}{\pi}\int_{-\infty}^{\infty} d\omega e^{-i\omega t}[n(\omega,T_\alpha)+1]\mathrm{Im}\chi_\alpha^{+-}(\mathbf{q},\omega), \tag{93}$$

and likewise in N, where $n(\omega, T_\alpha) = 1/[\exp(\hbar\omega/k_\mathrm{B}T_\alpha) - 1]$ is the Bose distribution function with effective temperature T_α, and α takes either F or N (α = F, N). Inserting Eqs. 92 and 93 into Eq. 91, the interface spin current is expressed as

$$\begin{aligned} J_{F/N}^{s} &= \frac{2\hbar}{\pi}N_I J_{\mathrm{eff}}^2 \sum_{\mathbf{p},\mathbf{q}} \int_{-\infty}^{\infty} d\omega[n(\omega,T_\mathrm{m}) - n(\omega+\delta\mu/\hbar,T_e)] \\ &\times \mathrm{Im}\chi_\mathrm{F}^{+-}(\mathbf{q},\omega)\mathrm{Im}\chi_\mathrm{N}^{+-}(\mathbf{p},\omega+\delta\mu/\hbar), \end{aligned} \tag{94}$$

where $T_\mathrm{m}(= T_\mathrm{F})$ is the magnon temperature and $T_\mathrm{e}(= T_\mathrm{N})$ is the conduction-electron temperature. The conduction electrons quickly equilibrate with the lattice, so that T_e is equal to the lattice (phonon) temperature T_p. Using $\chi_\mathrm{F}^{+-}(\mathbf{q},\omega) = 2\langle S_z\rangle/\left(\hbar\omega - \hbar\omega_\mathbf{q} + i\delta\right)$ for the localized moments without damping, where $\hbar\omega_\mathbf{q}$ is the magnon excitation energy, and $\chi_\mathrm{N}^{+-}(\mathbf{p},\omega) = \sum_\mathbf{k}\left[f(\xi_\mathbf{k}) - f\left(\xi_{\mathbf{k}+\mathbf{p}}\right)\right]/\left(\hbar\omega - \xi_\mathbf{k} + \xi_{\mathbf{k}+\mathbf{p}} + i\delta\right)$ for the conduction electrons, where $f(\xi_\mathbf{k})$ is the Fermi distribution function and $\xi_\mathbf{k}$ is one-electron energy measured from the Fermi level, the interface spin current becomes [51]

$$\begin{aligned} J_{\mathrm{F/N}}^{s} &= 4\pi A_\mathrm{J}\frac{\langle S_z\rangle}{a^2}\left(\frac{J_{sd}}{\varepsilon_\mathrm{F}}\right)^2\frac{1}{N_S} \\ &\times\sum_\mathbf{q}\left(\hbar\omega_\mathbf{q}+\delta\mu\right)\left[\coth\left(\frac{\hbar\omega_\mathbf{q}+\delta\mu}{2k_\mathrm{B}T_\mathrm{e}}\right) - \coth\left(\frac{\hbar\omega_\mathbf{q}}{2k_\mathrm{B}T_\mathrm{m}}\right)\right]. \end{aligned} \tag{95}$$

Note that $J_{\mathrm{F/N}}^{s}$ vanishes in the equilibrium condition of $T_\mathrm{m} = T_\mathrm{e}$ and $\delta\mu = 0$.

To examine how the spin accumulation is converted to the magnon spin current and how the spin current depends on the magnon energy and temperature, one may consider a simple model that magnons have the parabolic dispersion with no excitation gap $\hbar\omega_\mathbf{q} = A_\mathrm{ex}q^2$. At high temperatures comparable to room temperature, Eq. 95 can be expanded up to the first order with respect to $\delta\mu$ and the temperature difference $T_\mathrm{m} - T_\mathrm{e}$, which leads to the spin-current density across the interface

$$j_{\mathrm{F/N}}^{\mathrm{s}} \approx -\frac{\hbar}{2e}\frac{G_{\uparrow\downarrow}^{(\mu)}}{2eA_\mathrm{J}}\delta\mu(0) - \frac{\hbar}{2e}\frac{G_{\uparrow\downarrow}^{(T)}}{2eA_\mathrm{J}}k_\mathrm{B}(T_\mathrm{m} - T_\mathrm{e}), \tag{96}$$

where the interface spin conductances normalized to $(2e^2/h)A_\mathrm{J}$ are

$$g_{\uparrow\downarrow}^{(\mu)} = \frac{G_{\uparrow\downarrow}^{(\mu)}}{(2e^2/h)A_\mathrm{J}} \approx 8\pi(6/\pi)^{1/3}\frac{\langle S_z\rangle}{a^2}\left(\frac{J_{sd}}{\varepsilon_\mathrm{F}}\right)^2\left(\frac{k_\mathrm{B}T_\mathrm{m}}{A_\mathrm{ex}}\right), \tag{97}$$

$$g_{\uparrow\downarrow}^{(T)} = \frac{G_{\uparrow\downarrow}^{(T)}}{(2e^2/h)A_{\mathrm{J}}} \approx 16\pi^2 \frac{\langle S_z \rangle}{a^2} \left(\frac{J_{sd}}{\varepsilon_{\mathrm{F}}}\right)^2, \tag{98}$$

which correspond to the so-called mixing conductance with dimensions of cm^{-2}.

It follows from the parameter values $\langle S_z \rangle = 5/2$, $a_S = 0.6$ nm, $A_{\mathrm{ex}} = 6.24$ meV nm^2, and $k_{\mathrm{B}}T \sim 26$ meV at room temperature that $g_{\uparrow\downarrow}^{(\mu)} \sim 3.5 \times 10^{16} (J_{sd}/\varepsilon_{\mathrm{F}})^2\,\mathrm{cm}^{-2}$ and $g_{\uparrow\downarrow}^{(T)} \sim 1.1 \times 10^{17} (J_{sd}/\varepsilon_{\mathrm{F}})^2\,\mathrm{cm}^{-2}$. For example, the value of $(J_{sd}/\varepsilon_{\mathrm{F}}) = 0.5$ yields $g_{\uparrow\downarrow}^{(\mu)} \sim 1 \times 10^{15}\,\mathrm{cm}^{-2}$ and $g_{\uparrow\downarrow}^{(T)} \sim 3 \times 10^{15}\,\mathrm{cm}^{-2}$, which are the same order of magnitude as those in metallic junctions [33, 50].

Taking into account the interface spin current in Eq. 96 in the spin-diffusion theory and using the boundary condition that spin currents are continuous at the interface, one obtains the spin current and spin accumulation in the normal-metal layer of thickness d_{N} [70],

$$\delta\mu(x) = 2e\rho_N \lambda_s j_{\mathrm{F/N}}^s \frac{\cosh[(x - d_{\mathrm{N}})/\lambda_s]}{\sinh(d_{\mathrm{N}}/\lambda_s)}, \tag{99}$$

$$j_{\mathrm{N}}^s(x) = -j_{\mathrm{F/N}}^s \frac{\sinh[(x - d_{\mathrm{N}})/\lambda_s]}{\sinh(d_{\mathrm{N}}/\lambda_s)}, \tag{100}$$

and the interface spin-current density which includes the thermal pumping and backflow effects,

$$j_{\mathrm{F/N}}^s = -\frac{1}{4\pi} g_{\uparrow\downarrow}^{(T)} \frac{k_{\mathrm{B}}(T_{\mathrm{m}} - T_{\mathrm{e}})}{1 + \left(g_{\uparrow\downarrow}^{(\mu)}/g_{\mathrm{N}}^s\right)\coth(d_{\mathrm{N}}/\lambda_s)}, \tag{101}$$

where $g_{\mathrm{N}}^s = (h/2e^2)/(\rho_{\mathrm{N}}\lambda_s)$ is the spin conductance of the N electrode.

The electric field induced by ISHE in the normal layer is given by $E_{\mathrm{ISHE}} = \theta_{\mathrm{SH}} \rho_{\mathrm{N}} (2e/\hbar) \langle j_{\mathrm{N}}^s(z) \rangle$, so that the detected voltage $V_{\mathrm{ISHE}} = w_{\mathrm{N}} E_{\mathrm{ISHE}}$ reads

$$V_{\mathrm{ISHE}} = -\theta_{\mathrm{SH}} \left(\frac{w_{\mathrm{N}}}{d_{\mathrm{N}}}\right) \frac{\left(g_{\uparrow\downarrow}^{(T)}/g_{\mathrm{N}}^s\right)\tanh(d_{\mathrm{N}}/2\lambda_s)}{1 + \left(g_{\uparrow\downarrow}^{(\mu)}/g_{\mathrm{N}}^s\right)\coth(d_{\mathrm{N}}/2\lambda_s)} \frac{k_{\mathrm{B}}}{e}(T_{\mathrm{m}} - T_{\mathrm{e}}), \tag{102}$$

which enables one to deduce the nonequilibrium temperature difference of the order of $(T_{\mathrm{m}} - T_{\mathrm{e}}) \sim 3 \times 10^{-4}$ K for the measured value of $V_{\mathrm{ISHE}} = 1.5\ \mu$V in a YIG/Pt device and the parameter values of $\theta_{\mathrm{SH}} \approx 0.01$, $w_{\mathrm{N}} = 4$ mm, $d_{\mathrm{N}} = 15$ nm, and $g_{\uparrow\downarrow}^{(T)}/g_{\mathrm{N}}^s = g_{\uparrow\downarrow}^{(\mu)}/g_{\mathrm{N}}^s = 0.01$ $(J_{sd}/\varepsilon_{\mathrm{F}} \sim 1)$.

Magnon Current, Magnon Accumulation, and Magnon Temperature

It is important to find a relation between the effective magnon temperature and the magnon accumulation generated by a temperature gradient in a ferromagnetic insulator (FI). In the presence of temperature gradient ∇T along z in FI (see Fig. 8), the magnon current j_{m} may flow according to the phenomenological equation

$$j_{\mathrm{m}} = -D_{\mathrm{m}} \nabla \delta n_{\mathrm{m}} + \mathcal{L}_{\mathrm{m}}(-\nabla T), \tag{103}$$

where D_{m} is the diffusion constant of magnons, $\mathcal{L}_{\mathrm{m}}$ is a coefficient, the first term is the contribution of nonequilibrium magnon accumulation δn_{m}, and the second term is the contribution driven by the temperature gradient. Since individual magnons carry spin angular momentum $-\hbar$, the magnon spin current is $j_{\mathrm{m}}^{s} = -\hbar j_{\mathrm{m}}$.

The magnon accumulation is

$$\delta n_{\mathrm{m}} = n_{\mathrm{m}} - \overline{n}_{\mathrm{m}}, \tag{104}$$

where $n_{\mathrm{m}} = (\hbar\gamma)^{-1}(M_s - M_z) = \sum_{\mathbf{q}} \left\langle b_{\mathbf{q}}^{\dagger} b_{\mathbf{q}} \right\rangle$ is the magnon population in a nonequilibrium state; $b_{\mathbf{q}}^{\dagger}(b_{\mathbf{q}})$ is the magnon creation (annihilation) operator; $\langle b_{\mathbf{q}}^{\dagger} b_{\mathbf{q}} \rangle$ is the distribution of magnon with energy $\hbar\omega_{\mathbf{q}}$, which is represented by the Bose distribution function with magnon temperature T_{m}; and $\overline{n}_{\mathrm{m}}$ is the local equilibrium magnon population with the lattice (phonon) temperature T_{p} which is equal to the applied temperature. At high temperatures around room temperature (RT), the magnon distribution functions can be expanded with respect to $\hbar\omega_{\mathbf{q}}/k_{\mathrm{B}}T_{\alpha}$, yielding

$$\delta n_{\mathrm{m}} \approx (6/\pi)^{1/3} \frac{k_{\mathrm{B}}}{2\pi A_{\mathrm{ex}} a_S} \left(T_{\mathrm{m}} - T_{\mathrm{p}}\right), \tag{105}$$

where $\sum_{\mathbf{q}} \left(\hbar\omega_{\mathbf{q}}\right)^{-1} = (6/\pi)^{1/3} V_{\mathrm{F}}/(2\pi A_{\mathrm{ex}} a_S)$ is used. Note that the magnon accumulation is represented by the temperature difference $T_{\mathrm{m}} - T_{\mathrm{p}}$, the deviation of the magnon temperature from the lattice temperature.

Assuming the continuity equation for magnons, $\nabla \cdot \mathbf{j}_{\mathrm{m}} = -\delta n_{\mathrm{m}}/\tau_{\mathrm{m}}$, where τ_{m} is the magnon relaxation time, and using Eq. 103, the magnon-diffusion equation is written as

$$\nabla^2 \delta n_{\mathrm{m}}(z) = \frac{1}{\lambda_{\mathrm{m}}^2} \delta n_{\mathrm{m}}(z), \tag{106}$$

where $\lambda_{\mathrm{m}} = \sqrt{D_{\mathrm{m}}\tau_{\mathrm{m}}}$ is the magnon-diffusion length. Using the boundary condition $\mathbf{j}_{\mathrm{m}} = 0$ at the sample ends of $z = \pm L/2$, the magnon spin current $\left(j_{\mathrm{m}}^{s} = -\hbar j_{\mathrm{m}}\right)$ and magnon accumulation become

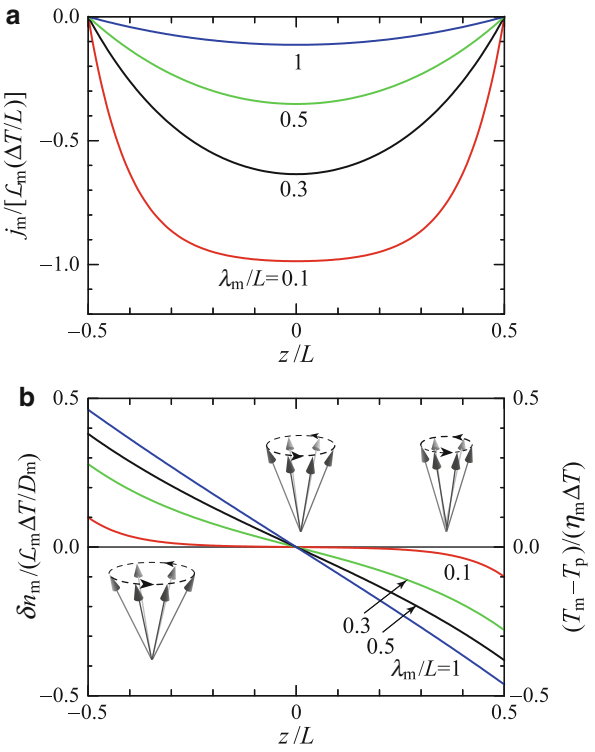

Fig. 7 (**a**) Spatial distribution of (**a**) magnon current and (**b**) magnon accumulation, which is proportional to the difference of magnon and lattice temperatures, in FI in the presence of a positive temperature gradient along $z(-L/2 < z < L/2)$

$$j_m^s(z) = -\hbar\left[1 - \frac{\cosh(z/\lambda_m)}{\cosh(L/2\lambda_m)}\right]\mathcal{L}_m(-\nabla T), \tag{107}$$

$$\delta n_m(z) = \frac{\lambda_m}{D_m}\left[\frac{\sinh(z/\lambda_m)}{\cosh(L/2\lambda_m)}\right]\mathcal{L}_m(-\nabla T). \tag{108}$$

When the temperature difference ΔT is applied between the ends of the sample with a linear temperature variation $T(z) = T_0 + (z/L)\Delta T$ along the z direction in a ferromagnetic insulator of length L, the temperature gradient is given by $\nabla T = \Delta T/L$. Equating Eqs. 105 and 108, the nonequilibrium magnon temperature varies along the temperature gradient as

$$T_m - T_p = -\eta_m \frac{\lambda_m}{L}\left[\frac{\sinh(z/\lambda_m)}{\cosh(L/2\lambda_m)}\right]\nabla T, \tag{109}$$

where $\eta_m = 2\pi(6/\pi)^{-1/3}(\mathcal{L}_m A_{ex} a_S/k_B D_m)$.

The spatial distributions of the magnon current and the magnon accumulation in the presence of temperature gradient are shown in Fig. 7a, b, respectively. Both magnon current and magnon accumulation are proportional to the difference between the magnon and lattice temperatures. The magnon (particle) current

flows from the high-T side to the low-T side and vanishes at the sample ends due to the boundary condition $j_{\rm m}(z = \pm L/2) = 0$. This magnon flow creates an accumulation of magnons in the low-T region, where the effective magnon temperature is higher than the lattice temperature, whereas it creates a depletion of magnons in the high-T region, where the effective magnon temperature is lower than the lattice temperature.

Spin Seebeck Effect

When a normal-metal layer is placed at position $z_{\rm N}$ on the FI layer as shown in Fig. 8a, the electron temperature of the N layer equilibrates with the lattice temperature of the FI layer at the contact position ($T_{\rm e} = T_{\rm p}$). Thus, from Eqs. 102 and 109, the inverse spin-Hall voltage generated by SSE becomes

$$V_{\rm ISHE} = \xi_{\rm m}\left(\frac{w_{\rm N}}{d_{\rm N}}\right)\left(\frac{k_{\rm B}\Delta T}{|e|}\right)\frac{\lambda_{\rm m}}{L}\left[\frac{\sinh(z_{\rm N}/\lambda_{\rm m})}{\cosh(L/2\lambda_{\rm m})}\right], \tag{110}$$

where

$$\xi_{\rm m} = \theta_{\rm SH}\eta_{\rm m}\frac{\left(g^{(T)}_{\uparrow\downarrow}/g^{s}_{\rm N}\right)\tanh(d_{\rm N}/2\lambda_s)}{1+\left(g^{(\mu)}_{\uparrow\downarrow}/g^{s}_{\rm N}\right)\coth(d_{\rm N}/\lambda_s)}. \tag{111}$$

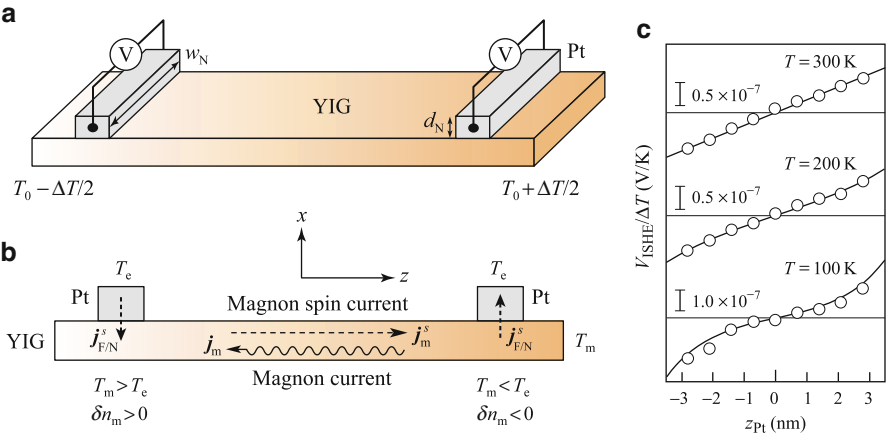

Fig. 8 (**a**) Schematic diagram of a device setup for measuring the spin Seebeck effect in the presence of temperature bias ΔT between the two ends of a YIG film. (**b**) Schematic illustration of magnon (particle) current $j_{\rm m}$, magnon spin current $j^s_{\rm m} = (-\hbar)j_{\rm m}$, and magnon accumulation $\delta n_{\rm m}$ in FI in the presence of temperature gradient $\Delta T/L$ along z. (**c**) Dependence of $V_{\rm ISHE}/\Delta T$ on the displacement $z_{\rm Pt}$ of Pt wire from the center of YIG layer along the z direction. The *open circles* are the experimental data by Uchida et al. [72] and the *solid curves* are the fitting results using Eq. 110

When the magnon-diffusion length is larger than the sample length ($\lambda_m > L$),

$$V_{ISHE} \approx \xi_m (w_N/d_N)(k_B \Delta T/|e|)(z_N/L), \tag{112}$$

indicating that V_{ISHE} varies linearly with respect to z_N, which has been observed in a YIG/Pt system at room temperature [72].

A qualitative physical picture of the spin Seebeck effect is presented in Fig. 8b. A nonequilibrium state between magnetic moments in YIG and conduction electrons in Pt is created by applying the temperature difference between the two ends of the YIG film. The thermally excited magnons flow from the high-T to the low-T ends driven by the temperature gradient. This magnon flow creates a magnon accumulation ($\delta n_m > 0$) in the low-T side, where the effective magnon temperature is higher than the lattice temperature ($T_m > T_p$), whereas it creates a magnon depletion ($\delta n_m < 0$) in the high-T side, where the effective magnon temperature is lower than the lattice temperature ($T_m < T_p$). Since the electron temperature T_e of the N layer equilibrates with the lattice temperature at the contact z_N ($T_e = T_p$), T_m is higher (lower) than T_e at the contact in the low-T (high-T) side [78]. When the contact lies in high-T side, the spin current flows from FI into N in proportion to $T_m - T_e$ and also to ΔT, whereas it flows in the reverse direction from N to FI when the contact lies in low-T side. Consequently, the voltage signal V_{ISHE} generated by the spin current has different signs depending on whether the contact position z_N is in the high-T or low-T region. Figure 8c shows the experimental date measured by Uchida et al. [72], and the solid curves are the fitting results using Eq. 110. The nearly linear dependence of measured V_{ISHE} at room temperature implies that the magnon-diffusion length is very long of the order of mm, and the damping of the magnon accumulation is extremely weak in YIG which prevents a rapid equilibration of magnons with phonons. The qualitative picture presented above is validated by the microscopic models based on scattering and linear-response theories [79, 80] and numerical simulations [81].

Thermally induced spin-angular-momentum transfer across the YIG/Pt interface has been used to control the Gilbert damping of magnetization [82].

Summary

In this chapter, a theoretical description for spin pumping from a ferromagnet into a normal metal is presented based on the spin-exchange interaction between localized moments and conduction electrons in hybrid nanostructures. It is demonstrated that pure spin currents are generated by the coherent spin pumping due to ferromagnetic resonance (FMR) and the thermal spin pumping due to the spin Seebeck effect (SSE). The inverse effect that the spin dynamics is manipulated by spin injection from a normal metal with strong spin-orbit coupling into a ferromagnet using the spin-Hall effect (SHE) is discussed. Owing to the spin-exchange interaction between localized moments and conduction electrons, the spin angular momentum is transferred from one subsystem where nonequilibrium electron spins or magnons

are accumulated as a spin source by means of FMR, SHE, or SSE to a neighboring nonmagnetic subsystem where a pure spin current carried by electron spins is generated to produce an electric current of conduction electrons (dc voltage) by means of the inverse spin-Hall effect (ISHE) or to a neighboring magnetic subsystem where magnon excitation or spin-transfer torque strongly affects the magnetization dynamics (damping) or even induces the magnetization switching. Spin pumping and related phenomena would open up new avenues in the field of metallic, semiconducting, and insulating spintronics.

The present formalism based on the spin-exchange interaction is an alternative to the spin-pumping formalism based on the Landauer-Büttiker scattering theory. While these approaches are apparently different and have been developed rather independently so far, these are two sides of the same coin and provide complementary views for spin pumping. Further intensive and comprehensive studies would provide a unified picture of spin pumping in hybrid nanostructures.

References

1. Maekawa S (ed) (2006) Concepts in spin electronics. Oxford University Press, Oxford
2. Tsymbal E, Zutić I (eds) (2011) Handbook of spin transport and magnetism. CRC Press, Boca Raton
3. Žutić I, Fabian J, Das Sarma S (2004) Spintronics: Fundamentals and applications. Rev Mod Phys 76:323
4. Maekawa S, Valenzuela SO, Saitoh E, Kimura T (eds) (2012) Spin current. Oxford University Press, Oxford
5. Johnson M, Silsbee RH (1985) Interfacial charge-spin coupling: Injection and detection of spin magnetization in metals. Phys Rev Lett 55:1790
6. Johnson M (1993) Spin accumulation in gold films. Phys Rev Lett 70:2142
7. Jedema FJ, Filip AT, van Wees BJ (2001) Electrical spin injection and accumulation at room temperature in an all-metal mesoscopic spin valve. Nature 410:345
8. Jedema FJ, Heersche HB, Filip AT, Baselmans JJA, van Wees BJ (2002) Electrical detection of spin precession in a metallic mesoscopic spin valve. Nature 416:713
9. Lou XH, Adelmann C, Crooker SA, Garlid ES, Zhang J, Reddy KSM, Flexner SD, Palmstrom CJ, Crowell PA (2007) Electrical detection of spin transport in lateral ferromagnet-semiconductor devices. Nat Phys 3:197
10. Han W, McCreary KM, Pi K, Wang WH, Li Y, Wen H, Chen JR, Kawakami RK (2012) Spin transport and relaxation in graphene. J Magn Magn Mater 324:369
11. Takahashi S, Maekawa S (2003) Spin injection and detection in magnetic nanostructures. Phys Rev B 67:052409
12. Silsbee RH, Janossy A, Monod P (1979) Coupling between ferromagnetic and conduction-spin-resonance modes at a ferromagnetic-normal-metal interface. Phys Rev B 19:4382
13. Mizukami S, Ando Y, Miyazaki T (2002) Effect of spin diffusion on Gilbert damping for a very thin permalloy layer in Cu/permalloy/Cu/Pt films. Phys Rev B 66:104413
14. Tserkovnyak Y, Brataas A, Bauer GEW (2002) Spin pumping and magnetization dynamics in metallic multilayers. Phys Rev Lett 88:117601
15. Costache MV, Sladkov M, Watts SM, van der Wal CH, van Wees BJ (2006) Electrical detection of spin pumping due to the precessing magnetization of a single ferromagnet. Phys Rev Lett 97:216603
16. Mosendz O, Pearson JE, Fradin FY, Bauer GEW, Bader SD, Hoffmann A (2010) Quantifying spin Hall angles from spin pumping: Experiments and theory. Phys Rev Lett 104:046601

17. Ando K, Takahashi S, Ieda J, Kurebayashi H, Trypiniotis T, Barnes CHW, Maekawa S, Saitoh E (2011) Electrically tunable spin injector free from the impedance mismatch problem. Nat Mater 10:655
18. Kato YK, Myers RC, Gossard AC, Awschalom DD (2004) Observation of the spin Hall effect in semiconductors. Science 306:1910
19. Wunderlich J, Kaestner B, Sinova J, Jungwirth T (2005) Experimental observation of the spin-Hall effect in a two-dimensional spin-orbit coupled semiconductor system. Phys Rev Lett 94:047204
20. Valenzuela SO, Tinkham M (2006) Direct electronic measurement of the spin Hall effect. Nature 442:176
21. Saitoh E, Ueda M, Miyajima H, Tatara G (2006) Conversion of spin current into charge current at room temperature: Inverse spin-Hall effect. Appl Phys Lett 88:182509
22. Kimura T, Otani Y, Sato T, Takahashi S, Maekawa S (2007) Room-temperature reversible spin Hall effect. Phys Rev Lett 98:156601
23. Seki T, Hasegawa Y, Mitani S, Takahashi S, Imamura H, Maekawa S, Nitta J, Takanasni K (2008) Giant spin Hall effect in a perpendicularly spin-polarized FePt/Au device. Nat Mater 7:125
24. D'yakonov MI, Perel' VI (1971) Current induced spin orientation of electrons in semiconductors. Phys Lett A 35:459
25. Hirsch JE (1999) Spin Hall effect. Phys Rev Lett 83:1834
26. Zhang S (2001) Spin Hall effect in the presence of spin diffusion. Phys Rev Lett 85:393
27. Murakami S, Nagaosa N, Zhang SC (2003) Dissipationless quantum spin current at room temperature. Science 301:1348–1351
28. Sinova J, Culcer D, Niu Q, Sinitsyn NA, Jungwirth T, MacDonald AH (2004) Universal intrinsic spin Hall effect. Phys Rev Lett 92:126603
29. Takahashi S, Maekawa S (2002) Hall effect induced by a spin-polarized current in superconductors. Phys Rev Lett 88:116601
30. Bauer GEW, Saitoh E, van Wees BJ (2012) Spin caloritronics. Nat Mater 11:391
31. Adachi H, Uchida K, Saitoh E, Maekawa S (2013) Theory of the spin Seebeck effect. Rep Prog Phys 76:036501
32. Tserkovnyak Y, Brataas A, Bauer GEW (2002) Spin pumping and magnetization dynamics in metallic multilayers. Phys Rev B 66:224403
33. Tserkovnyak Y, Brataas A, Bauer GEW, Halperin BI (2005) Nonlocal magnetization dynamics in ferromagnetic heterostructures. Rev Mod Phys 77:1375
34. Brataas A, Bauer GEW, Kelly PJ (2006) Non-collinear magnetoelectronics. Phys Rep 427:157
35. Büttiker M, Thomas H, Prétre A (1994) Current partition in multiprobe conductors in the presence of slowly oscillating external potentials. Z Phys B 94:133
36. Brouwer PW (1998) Scattering approach to parametric pumping. Phys Rev B 58:R10135
37. Šimánek E, Heinrich B (2003) Gilbert damping in magnetic multilayers. Phys Rev B 67:144418
38. Mills DL (2003) Ferromagnetic resonance relaxation in ultrathin metal films: The role of the conduction electrons. Phys Rev B 68:014419
39. Zhang S, Li Z (2003) Roles of nonequilibrium conduction electrons on the magnetization dynamics of ferromagnets. Phys Rev Lett 93:127204
40. Takeuchi A, Hosono K, Tatara G (2010) Diffusive versus local spin currents in dynamic spin pumping systems. Phys Rev B 81:144405
41. Yosida K (1998) Theory of magnetism. Springer, Berlin, p 228
42. Gilbert TL (1955) A Lagrangian formulation of the gyromagnetic equation of the magnetic field. Phys Rev 100:1243
43. Bloch F (1946) Nuclear induction. Phys Rev 70:460
44. Torrey HC (1956) Bloch equations with diffusion terms. Phys Rev 104:563
45. Heinrich B, Tserkovnyak Y, Woltersdorf G, Brataas A, Urban R, Bauer GEW (2003) Dynamic exchange coupling in magnetic bilayers. Phys Rev Lett 90:187601

46. Takahashi S (2014) Giant enhancement of spin pumping in the out-of-phase precession mode. Appl Phys Lett 104:052407
47. Mizukami S, Ando Y, Miyazaki T (2001) The study on ferromagnetic resonance linewidth for NM/80NiFe/NM (NM=Cu, Ta, Pd and Pt) films. Jpn J Appl Phys 40:580
48. Azevedo A, Vilela-Leao LH, Rodriguez-Suarez RL, Santos AFL, Rezende SM (2011) Spin pumping and anisotropic magnetoresistance voltages in magnetic bilayers: Theory and experiment. Phys Rev B 83:144402
49. Nakayama H, Ando K, Harii K, Yoshino T, Takahashi R, Kajiwara Y, Uchida K, Fujikawa Y, Saitoh E (2012) Geometry dependence on inverse spin Hall effect induced by spin pumping in Ni_{81}Fe_{19}/Pt films. Phys Rev B 85:144408
50. Czeschka FD, Dreher L, Brandt MS, Weiler M, Althammer M, Imort IM, Reiss G, Thomas A, Schoch W, Limmer W, Huebl H, Gross R, Goennenwein STB (2011) Scaling behavior of the spin pumping effect in ferromagnet-platinum bilayers. Phys Rev Lett 107:046601
51. Takahashi S, Saitoh E, Maekawa S (2010) Spin current through a normal-metal/insulating-ferromagnet junction. J Phys Conf Ser 200:062030
52. Kajiwara Y, Harii K, Takahashi S, Ohe J, Uchida K, Mizuguchi M, Umezawa H, Kawai H, Ando K, Takanashi K, Maekawa S, Saitoh E (2010) Transmission of electrical signals by spin-wave interconversion in a magnetic insulator. Nature 464:262
53. Kajiwara Y, Takahashi S, Maekawa S, Saitoh E (2011) Detection of spin-wave spin current in a magnetic insulator. IEEE Trans Magn 47:1591
54. Castel V, Vlietstra N, Youssef JB, van Wees BJ (2012) Platinum thickness dependence of the inverse spin-Hall voltage from spin pumping in a hybrid yttrium iron garnet/platinum system. Appl Phys Lett 101:132414
55. Weiler M, Althammer M, Schreier M, Lotze J, Pernpeintner M, Meyer S, Huebl H, Gross R, Kamra A, Xiao J, Chen YT, Jiao H, Bauer GEW, Goennenwein STB (2013) Experimental test of the spin mixing interface conductivity concept. Phys Rev Lett 111:176601
56. Heinrich B, Burrowes C, Montoya E, Kardasz B, Girt E, Song YY, Sun Y, Wu M (2011) Spin pumping at the magnetic insulator (YIG)/normal metal (Au) interfaces. Phys Rev Lett 107:066604
57. Jia X, Liu K, Xia K, Bauer GEW (2011) Spin transfer torque on magnetic insulators. Eur Phys Lett 96:17005
58. Ando K, Takahashi S, Harii K, Sasage K, Ieda J, Maekawa S, Saitoh E (2008) Electric manipulation of spin relaxation using the spin Hall effect. Phys Rev Lett 101:036601
59. Liu L, Moriyama T, Ralph DC, Buhrman RA (2011) Spin-torque ferromagnetic resonance induced by the spin Hall effect. Phys Rev Lett 106:036601
60. Kondou K, Sukegawa H, Mitani S, Tsukagoshi K, Kasai S (2012) Evaluation of spin Hall angle and spin diffusion length by using spin current-induced ferromagnetic resonance. Appl Phys Express 5:073002
61. Liu L, Pai CF, Li Y, Tseng HW, Ralph DC, Buhrman RA (2012) Spin-torque switching with the giant spin Hall effect of Tantalum. Science 336:555
62. Slonczewski JC (1996) Current-driven excitation of magnetic multilayers. J Magn Magn Mater 159:L1
63. Petit S, Baraduc C, Thirion C, Ebels U, Liu Y, Li M, Wang P, Dieny B (2007) Spin-torque influence on the high-frequency magnetization fluctuations in magnetic tunnel junctions. Phys Rev Lett 98:077203
64. Ando K, Takahashi S, Ieda J, Kajiwara Y, Nakayama H, Yoshino T, Harii K, Fujikawa Y, Matsuo M, Maekawa S, Saitoh E (2011) Inverse spin-Hall effect induced by spin pumping in metallic system. J Appl Phys 109:103913
65. Mosendz O, Vlaminck V, Pearson JE, Fradin FY, Bauer GEW, Bader SD, Hoffmann A (2010) Detection and quantification of inverse spin Hall effect from spin pumping in permalloy/normal metal bilayers. Phys Rev B 82:214403
66. Valet T, Fert A (1993) Theory of the perpendicular magnetoresistance in magnetic multilayers. Phys Rev B 48:7099

67. Takahashi S, Imamura H, Maekawa S (2006) Spin injection and spin transport in hybrid nanostructures. In: Maekawa S (ed) Concept in spin electronics. Oxford University Press, Oxford
68. Takahashi S, Maekawa S (2008) Spin current in metals and superconductors. J Phys Soc Jpn 77:031009
69. Takahashi S, Maekawa S (2008) Spin current, spin accumulation and spin Hall effect. Sci Technol Adv Mater 9:014105
70. Takahashi S, Maekawa S (2011) Spin transport in hybrid nanostructures. In: Tsymbal E, Zutić I (eds) Handbook of spin transport and magnetism. CRC Press, Boca Raton
71. Uchida K, Takahashi S, Harii K, Ieda J, Koshibae W, Ando K, Maekawa S, Saitoh E (2008) Observation of the spin Seebeck effect. Nature 455:778
72. Uchida K, Xiao J, Adachi H, Ohe J, Takahashi S, Ieda J, Ota T, Kajiwara Y, Umezawa H, Kawai H, Bauer GEW, Maekawa S, Saitoh E (2010) Spin Seebeck insulator. Nat Mater 9:894
73. Jaworski CM, Yang J, Mack S, Awschalom DD, Heremans JP, Myers RC (2010) Observation of the spin-Seebeck effect in a ferromagnetic semiconductor. Nat Mater 9:898
74. Kirihara A, Uchida K, Kajiwara Y, Ishida M, Nakamura Y, Manako T, Saitoh E, Yorozu S (2011) Spin-current-driven thermoelectric coating. Nat Mater 11:686
75. Wang Z, Sun Y, Wu M, Tiberkevich V, Slavin A (2011) Control of spin waves in a thin film ferromagnetic insulator through interfacial spin scattering. Phys Rev Lett 107:146602
76. Mahan GD (2000) Many particle physics. Kluwer Academic/Plenum, New York
77. Rammer J (2004) Quantum transport theory. Westview Press, Boulder, p 305
78. Sanders DJ, Watson D (1977) Effect of magnon-phonon thermal relaxation on heat transport by magnons. Phys Rev B 15:1489
79. Xiao J, Bauer GEW, Uchida K, Saitoh E, Maekawa S (2010) Theory of magnon-driven spin Seebeck effect. Phys Rev B 81:214418
80. Adachi H, Ohe J, Takahashi S, Maekawa S (2011) Linear-response theory of spin Seebeck effect in ferromagnetic insulators. Phys Rev B 83:094410
81. Ohe J, Adachi H, Takahashi S, Maekawa S (2011) Numerical study on the spin Seebeck effect. Phys Rev B 83:115118
82. Lu L, Sun Y, Jantz M, Wu M (2012) Control of ferromagnetic relaxation in magnetic thin films through thermally induced interfacial spin transfer. Phys Rev Lett 108:257202